ACS Energy LETTERS

http://pubs.acs.org/journal/aelccp

Electrochemically Induced CO_2 Capture Enabled by Aqueous Quinone Flow Chemistry

Yan Jing,[▽] Kiana Amini,[▽] Dawei Xi, Shijian Jin, Abdulrahman M. Alfaraidi, Emily F. Kerr, Roy G. Gordon,* and Michael J. Aziz*

Cite This: *ACS Energy Lett.* 2024, 9, 3526−3535

Read Online

ACCESS | Metrics & More | Article Recommendations | Supporting Information

ABSTRACT: Electrochemically driven CO_2 capture processes utilizing redox-active organics in aqueous flow chemistry show promise for nonflammability, continuous-flow engineering and the possibility of being driven at a high current density by inexpensive, clean electricity. We show that deprotonated hydroquinone−CO_2 adducts, whose insolubility limits the utility of the quinone−hydroquinone redox couple, become soluble when alkylammonium cations are introduced. Consequently, we introduced alkylammonium groups to anthraquinone via covalent bonds, making the resulting bis[3-(trimethylammonio)propyl]-anthraquinones (BTMAPAQs) soluble. We report the first aqueous quinone flow chemistry-enabled electrochemical CO_2 capture/release process, which occurs at ambient temperature and pressure, and show that it proceeds via both pH-swing and nucleophilicity-swing mechanisms. 1,5-BTMAPAQ reaches the theoretical capture capacity of two CO_2 molecules per quinone from 1-bar CO_2−N_2 mixtures, for which the CO_2 partial pressure is as low as 0.05 bar, or the applied current density is as high as 100 mA/cm^2, or the organic concentration is as high as 0.4 M. The energetic cost ranges from 48 to 140 kJ/mol CO_2. In a crude simulated flue gas composed of 3% O_2, 10% CO_2, and 87% N_2, 1,5-BTMAPAQ electrolyte reversibly captured and released 50% of the theoretical capacity during an exposure of over 4 h. It outperforms its isomeric counterparts 1,4-, and 1,8-BTMAPAQ in capture capacity and O_2 tolerance, demonstrating a substituent position effect on the reactivity of isomers with CO_2 and O_2. The results provide fundamental insight into electrochemical CO_2 capture with aqueous quinone flow chemistry and suggest that the oxygen tolerance of reduced quinones may be significantly advanced through molecular engineering.

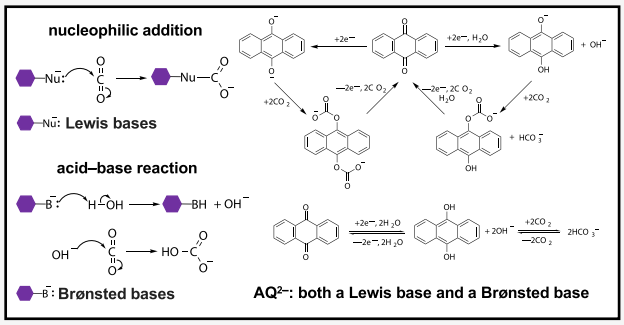

Accumulating atmospheric CO_2 concentrations from anthropogenic emissions is the major source of global climate change. While progress is being made in switching from fossil fuel combustion to virtually emissions-free electricity sources, hard-to-abate sectors such as aviation and shipping will remain large sources of emissions for decades, even in the most optimistic scenarios. Consequently, CO_2 removal—whether by capture from combustion exhaust or directly from the air or the ocean—is the subject of greatly increased attention, as it has become urgent to develop techniques that can be scaled up in a timely manner and globally deployed in the real world at reasonably low material and energetic costs.[1] Even after the attainment of a net zero emissions economy, it is likely that CO_2 removal will be desired in order to cut atmospheric concentrations toward preindustrial levels. In an increasingly electrified society, electrochemically driven CO_2 capture at ambient conditions becomes an increasingly attractive option.[2−5]

Quinones are ubiquitous electron-transfer carriers found in a range of living organisms.[6,7] Featuring structural diversity, richness, and tunability as well as the earth-abundance of the compositional elements (C, H, O, N, S), quinones have been used as industrial dyes and for large-scale industrial production of hydrogen peroxide.[8,9] Aqueous quinone flow batteries are approaching commercialization as a new generation of large-scale energy storage devices.[10] Apart from energy storage, it has been reported that quinone cores can also be utilized for electrochemically induced carbon capture via two different mechanisms, depending on the use of solvents (Figure 1a). First, CO_2 can be directly chemisorbed by reduced quinones

Received: May 6, 2024
Revised: June 2, 2024
Accepted: June 7, 2024
Published: June 28, 2024

https://doi.org/10.1021/acsenergylett.4c01235
ACS Energy Lett. 2024, 9, 3526−3535

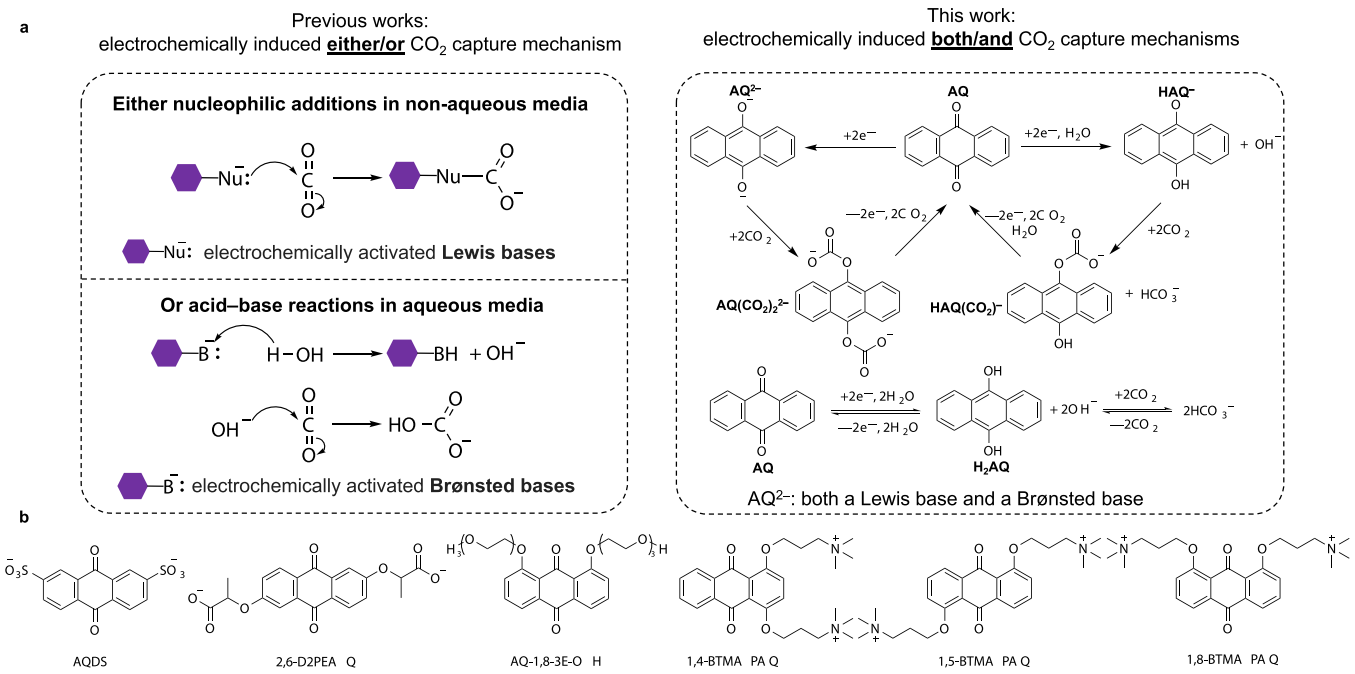

Figure 1. (a) In previous works, electrochemical CO_2 capture in nonaqueous media is driven by electrochemically activated Lewis bases (nucleophiles) which undergo nucleophilic additions with CO_2;[18,20,21,27] electrochemical CO_2 capture in aqueous media is driven by electrochemically activated Brønsted bases which undergo proton-coupled electron transfer induced acid−base reactions.[16,17,24,25,28,29,35,36] In this work, electrochemical CO_2 capture with aqueous anthraquinone solutions is driven by AQ^{2-}, which is both a Lewis base and a Brønsted base. The electrochemical CO_2 capture and release cycle involves both nucleophilicity- and pH-swing. (b) Six anthraquinone candidates that are soluble at neutral pH. Screened molecules: AQDS, 2,6-D2PEAQ, and AQ-1,8-3E-OH. Redesigned molecules: 1,4-, 1,5-, and 1,8-BTMAPAQ.

(Q^{2-}), forming adducts [$Q(CO_2)_2^{2-}$] in aprotic solvents.[11,12] Second, quinones can undergo proton-coupled electron transfer (PCET) to be reduced to the hydroquinone form (H_2Q) in protic solvents,[13−15] accompanied by the accumulation of hydroxide ions, indirectly leading to chemisorption of CO_2.[16,17] For both mechanisms, the captured CO_2 can be reversibly released upon electrochemical oxidation. For simplicity, we name the first (direct) capture mechanism the nucleophilicity-swing mechanism and the second (indirect) capture mechanism the pH-swing mechanism. In both cases, a CO_2 capture−release cycle involves quinone reduction (an electron transfer process, abbreviated as *E*: $Q + 2e^- \rightarrow Q^{2-}$; $Q + 2e^- + H_2O \rightarrow HQ^- + OH^-$; $Q + 2e^- + 2H_2O \rightarrow H_2Q + 2OH^-$), CO_2 absorption (a chemical reaction, abbreviated as *C*: $Q^{2-} + CO_2 \rightarrow Q(CO_2)_2^{2-}$; $HQ^- + CO_2 \rightarrow HQ(CO_2)^-$; $OH^- + CO_2 \rightarrow HCO_3^-$), and concerted electrochemical oxidation and CO_2 release (*E*: $Q(CO_2)_2^{2-} \rightarrow Q + 2CO_2 + 2e^-$; $HQ(CO_2)^- + HCO_3^- \rightarrow Q + H_2O + 2CO_2 + 2e^-$; $H_2Q + 2HCO_3^- \rightarrow Q + 2CO_2 + 2H_2O + 2e^-$). Therefore, both mechanisms undergo *ECE* processes in principle.

Quinones explored for CO_2 capture have been, almost without exception, immobilized on electrodes[18−21] or dissolved in organic electrolytes.[18,22,23] Solution-based capture inherits many of the advantages of flow batteries, including simple maintenance/top-off of active species, decoupled electrolyte activation and CO_2 capture, and continuous-flow engineering.[23−27] In particular, aqueous electrolytes possess the advantage[16,17,28−31] that water is nonflammable with virtually no cost; furthermore, high ionic conductivity of aqueous electrolytes allows high current density, enabling high areal throughput at ambient temperature and pressure. Combined, these advantages illustrate the opportunity for a capture system based on electrochemically driven aqueous-soluble quinone flow chemistry. The sole aqueous-soluble quinone studied to date for CO_2 capture, disodium 4,5-dihydroxy-1,3-benzenedisulfonate (tiron), was studied only in static H-cells.[15,32] One CO_2 per quinone was released via pH-swing caused by the electrochemical oxidization of tiron. Unfortunately, more than 60% of the initial capacity was lost after the first cycle due to the instability of the oxidized tiron molecule, which undergoes Michael addition and subsequent polymerization. To our knowledge, aqueous quinone flow chemistry-enabled electrochemical CO_2 capture and release has not previously been demonstrated.

Theoretically, to utilize a quinone for the PCET-mediated electrochemical CO_2 capture cycle in aqueous electrolyte, the initial pH of the quinone electrolytes should be somewhat below the pK_{a1} of H_2CO_3 (∼6), so that bicarbonate and carbonate concentrations are negligible compared to that of CO_2(aq). Upon electrochemical reduction, the quinone undergoes a PCET process, increasing the electrolyte pH until it reaches the pK_{a2} of the corresponding H_2Q; upon further reduction of the electrolyte, the quinone undergoes zero-proton, two-electron transfer, generating Q^{2-} dianions without further altering the electrolyte pH.[13,33] Because H_2Qs are weak acids and their pK_a values are usually less than 13,[13,33,34] concentrated quinone electrolytes, when reduced, are expected to be predominantly in dianionic form rather than H_2Q form, favoring nucleophilicity-swing carbon capture. The two OH^- ions generated from the formation of hydroquinones would capture one or two CO_2 molecules via carbonate ($2OH^- + CO_2 \rightarrow H_2O + CO_3^{2-}$) or bicarbonate ($OH^- + CO_2 \rightarrow HCO_3^-$) formation. The two oxygen sites on the dianionic form of the reduced quinone can each bind one CO_2 molecule,

https://doi.org/10.1021/acsenergylett.4c01235
ACS Energy Lett. 2024, 9, 3526−3535

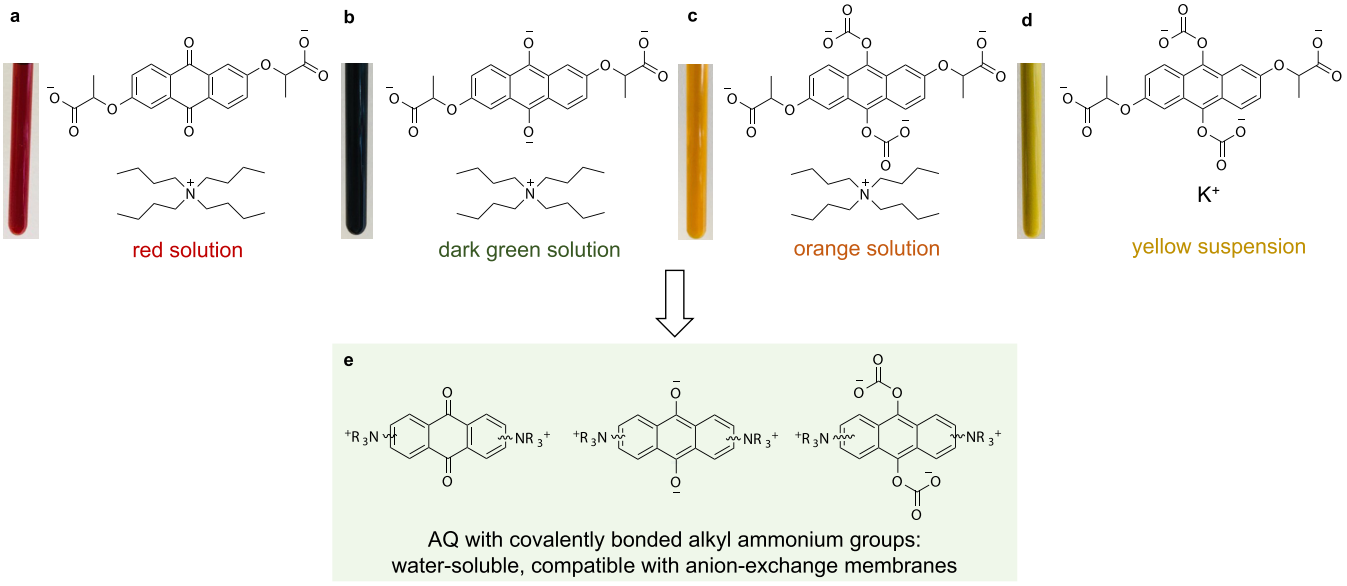

Figure 2. Effect of supporting salt cations on the solubility of $Q(CO_2)_2^{2-}$: (a) 0.1 M 2,6-D2PEAQ in 1 M TBACl; (b) 0.1 M reduced 2,6-D2PEAQ in 1 M TBACl; (c) 0.1 M reduced 2,6-D2PEAQ with saturated CO_2 in 1 M TBACl; (d) 0.1 M reduced 2,6-D2PEAQ with saturated CO_2 in 1 M KCl. (e) AQ possessing alkylammonium ending groups connected via covalent bonds, enhancing aqueous solubility and affording compatibility with anion-exchange membranes.

yielding either QCO_2^{2-} or $Q(CO_2)_2^{2-}$. Therefore, the CO_2 capture capacity of aqueous quinones is expected to range up to 2 CO_2 per quinone.

In general, aqueous quinones should meet several major criteria if they are to be used for electrochemical CO_2 capture. First, quinones should have high aqueous solubility in all states within their operational pH range. Second, the CO_2-reactive reduced species, including H_2Q, HQ^-, Q^{2-}, and $HQ(CO_2)^-$, and $Q(CO_2)_2^{2-}$, should resist reaction with O_2 long enough for most of the CO_2 capture capacity to be realized. Additionally, for the adduct formation mechanism, the rate constants should be reasonably high and the binding constants should be high enough for most of the maximum capture capacity of 2 CO_2 per quinone to be attained, but not so high as to lead to unnecessarily large adduct oxidation potentials.

Informed by a decade of endeavors in developing aqueous anthraquinone flow batteries,[37−39] we selected three anthraquinone derivatives that are aqueous-soluble at neutral pH: 2,7-disulfonated anthraquinone (AQDS),[40] 1,8-bis(2-(2-(2-hydroxyethoxy)ethoxy)ethoxy)anthracene-9,10-dione (AQ-1,8-3E-OH),[33] and 2,2′-((9,10-dioxo-9,10-dihydroanthracene-2,6-diyl)bis(oxy))dipropionic acid (2,6-D2PEAQ)[41] (Figure 1b). Although those quinones show >1.0 M aqueous solubility in both oxidized and reduced states when used in flow batteries, bright yellow precipitates formed when CO_2 was introduced to the reduced electrolytes. The yellow precipitates did not form and clear solutions were afforded when tetraalkylammonium chlorides were used as the supporting salts (Figure 2, Table S1). Specifically, substituting 1 M NaCl with 1 M tetramethylammonium chloride (TMACl) as the supporting salt in 0.1 M AQDS electrolyte (Figure S1), or replacing 1 M KCl with 1 M tetrabutylammonium chloride (TBACl) as the supporting salt in 0.1 M 2,6-D2PEAQ (Figure 2) or in 0.1 M AQ-1,8-3E-OH electrolytes, produces transparent, bright yellow solutions. One plausible explanation is that the bulky, amphiphilic tetraalkylammonium cations and $Q(CO_2)_2^{2-}$ form loose ion pairs rather than the tight ion pairs formed between alkali metal cations and $Q(CO_2)_2^{2-}$.[42] With the increased distance between $Q(CO_2)_2^{2-}$ and alkylammonium cations, the Coulomb attraction between the charges decreases, thereby raising the lattice energy and enhancing the aqueous solubility.[43] However, the bulkiness of tetraalkylammonium cations causes extremely high cell resistance (Figure S2a) in the flow cell systems because, in such cells, cation-exchange membranes must be used, resulting in a prohibitively high energetic cost.

Inspired by the observation of dramatic change in aqueous solubility of reduced AQs in the presence of CO_2 caused by tetraalkylammonium salts (Figure 2, Table S1), we hypothesized that anthraquinone derivatives tethered with bulky alkylammonium cations via covalent bonds might not only have high aqueous solubility in all states but also be compatible with anion-exchange membranes: the oxidized forms are positively charged and the reduced forms are charge-neutral but large in size, with correspondingly low expected crossover rates. We designed and synthesized 1,4-, 1,5-, 1,8-,[44] and 2,6-bis[3-(trimethylammonio)propyl]anthraquinones (BTMAPAQs), in which the numbers represent the positions of water-solubilizing chains (TMAP) bonded to the anthraquinone (AQ) core. Of the four isomers, 2,6-BTMAPAQ exhibits very limited solubility (<0.1 M) even in its oxidized state (Table S1); 1,8-BTMAPAQ$(CO_2)_2^{2-}$ becomes soluble when TBA^+ is used as the supporting salt cation (Figure S3); 1,4- and 1,5-BTMAPAQs are soluble in all states even if KCl is used as the supporting salt. Therefore, 1,4-, 1,5-, and 1,8-BTMAPAQs (Figure 1b) were investigated for electrochemical CO_2 capture.

Cyclic voltammetry (CV) was employed to investigate BTMAPAQs in buffered and unbuffered solutions. As shown in Figure 3a, at pH 7 in N_2, 1,5-BTMAPAQ exhibits a redox potential of −0.465 V vs SHE, with a peak separation of 90 mV. When the solution was constantly purged with CO_2, the major cathodic peak appears at −0.51 V, along with a minor cathodic peak at −0.28 V (Figure 3a), which might be caused by a CO_2 buffering effect, enabling 1,5-BTMAPAQ to partially undergo a PCET process.[13] The anodic peak of 1,5-

https://doi.org/10.1021/acsenergylett.4c01235
ACS Energy Lett. 2024, 9, 3526−3535

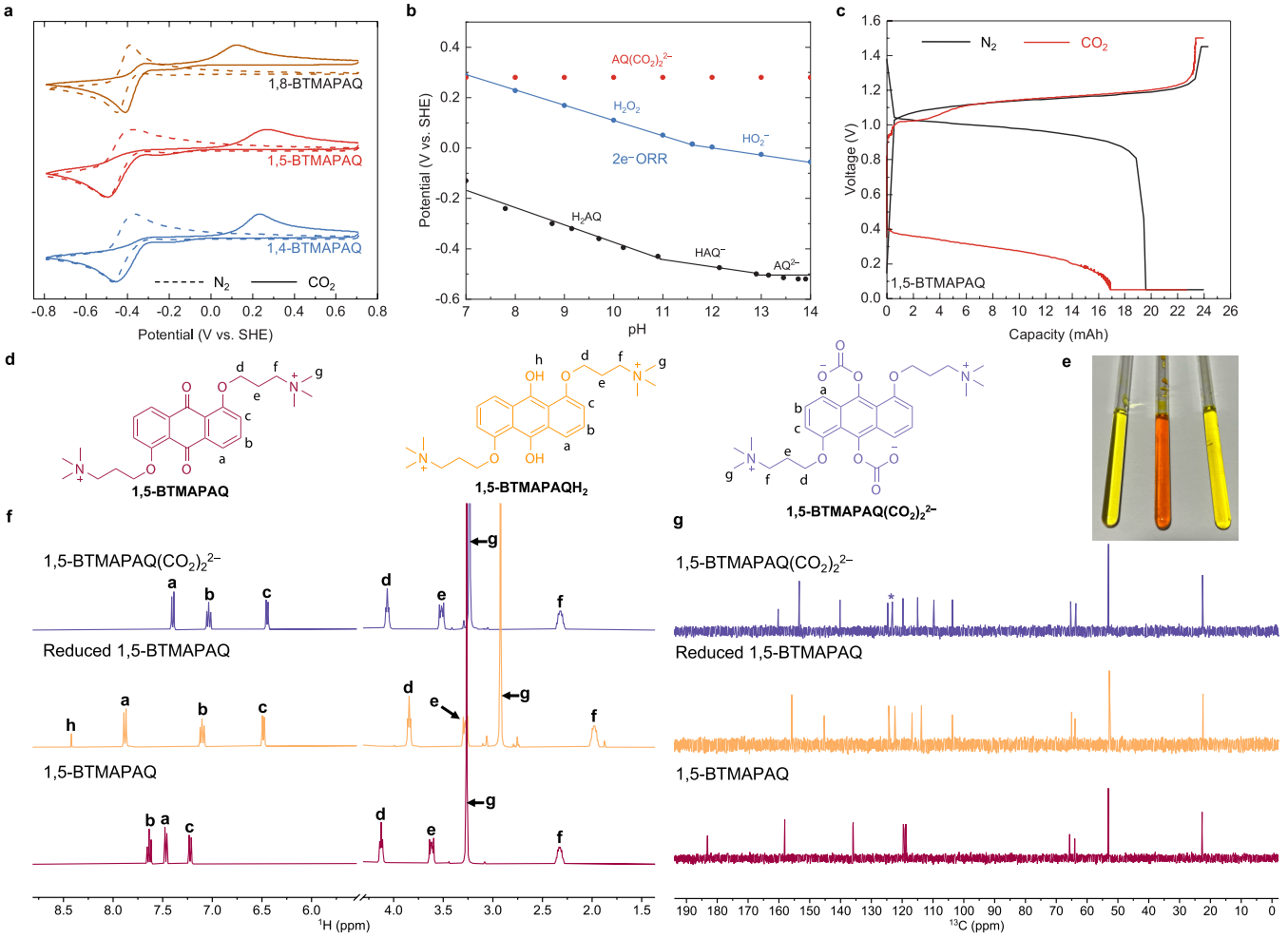

Figure 3. Electrochemical and physiochemical characterization of BTMAPAQ in N_2 and CO_2. (a) Cyclic voltammograms of 10 mL of 5 mM 1,4- and 1,5-BTMAPAQs in 1 M KCl or 5 mM 1,8-BTMAPAQ in 1 M KCl under streams of pure N_2 (dashed) or CO_2 (solid) at a scan rate of 100 mV s^{-1}. (b) Pourbaix diagrams of 1,5-BTMAPAQ ($AQ + 2e^- + 2H_2O \rightarrow H_2AQ + 2OH^-$; $AQ + 2e^- + H_2O \rightarrow HAQ^- + OH^-$; $AQ + 2e^- \rightarrow AQ^{2-}$) and 2-electron oxygen reduction reaction ($^1/_2O_2 + 2e^- + H_2O \rightarrow H_2O_2$; $1/2O_2 + 2e^- + H_2O \rightarrow HO_2^- + H^+$). (c) Voltage profiles of 1,5-BTMAPAQ | FcNCl in 100% N_2 (black) and 10% CO_2 + 90% N_2 (red). During the charge−discharge process, a constant current density of 20 mA/cm^2 was first applied until the voltages approached the preset cutoffs. Potential holds were applied at 1.45 V for the charge in pure N_2, 1.5 V for the charge in 90% N_2 and 10% CO_2, and 0.05 V for the discharge until the current density decreased to 1 mA/cm^2. (d) Structures of 1,5-BTMAPAQ, 1,5-BTMAPAQH_2, and 1,5-BTMAPAQ$(CO_2)_2^{2-}$. (e) NMR specimens, from left to right in the same order as the molecular structures in (d), and their ^{1}H NMR (f) and ^{13}C NMR (g) spectra. Note that ^{1}H NMR peak broadening was initially observed from the electrochemically reduced aqueous quinone due to the occurrence of residual radicals, but addition of a tiny amount of HCl afforded well-defined peak splitting in the aromatic region (panel f, orange). The chemical shift at 124.6 ppm in 1,5-BTMAPAQ$(CO_2)_2^{2-}$ (panel g, purple, identified with asterisk) is from the dissolved CO_2.[45]

BTMAPAQ largely shifts to +0.28 V, suggesting that extra energy is required to trigger electrochemical oxidation: 1,5-BTMAPAQ$(CO_2)_2^{2-}$ → 1,5-BTMAPAQ + $2CO_2$ + $2e^-$. Similar electrochemical behaviors were also shown by 1,4- and 1,8-BTMAPAQs.

To extract the relationship between the redox potentials of 1,5-BTMAPAQ and electrolyte pH, we ran CVs in a series of buffered electrolytes to plot its Pourbaix diagram (Figure 3b). The pK_{a1} and pK_{a2} of 1,5-BTMAPH_2AQ are estimated at 10.9 and 12.8, consistent with those of other aqueous-soluble anthrahydroquinones (H_2AQ).[33,34,41] Because of the dominance of the nucleophilicity-swing mechanism in concentrated solutions, hereafter the oxidized, reduced, and CO_2-bonded states of quinones are abbreviated as Q, Q^{2-}, and $Q(CO_2)_2^{2-}$.

We assembled BTMAPAQs | (ferrocenylmethyl)trimethylammonium chloride (FcNCl)[46] flow cells separated by anion-exchange membranes. Thanks to the compatibility between membrane and electrolytes, the alternating current area-specific resistance of the cells, measured via high-frequency electrochemical impedance spectroscopy, is as low as ∼1.5 Ω cm^2 (Figure S4). While operating in 0.1 bar of CO_2 and 0.9 bar of N_2, we noticed a distinct discharge voltage decrease (Figure 3c, Figure S5), consistent with the anodic peak shifts in CVs (Figure 3a), confirming that $Q(CO_2)_2^{2-}$ is the major product when the reduced form is exposed to CO_2. Interestingly, the color of the BTMAPAQ solution changed dramatically in different states. For instance, the 1,5-BTMAPAQ solution turned from bright yellow to light orange to pale yellow, corresponding to 1,5-BTMAPAQ, 1,5-BTMAPAQ^{2-}, and 1,5-BTMAPAQ$(CO_2)_2^{2-}$ (Figure 3e); the structure change was reflected by the distinct chemical shifts in both ^{1}H and ^{13}C NMR spectra (Figure 3f, g). Dramatic color changes as well as distinct chemical shifts were also exhibited by AQDS and 1,8-

https://doi.org/10.1021/acsenergylett.4c01235
ACS Energy Lett. 2024, 9, 3526−3535

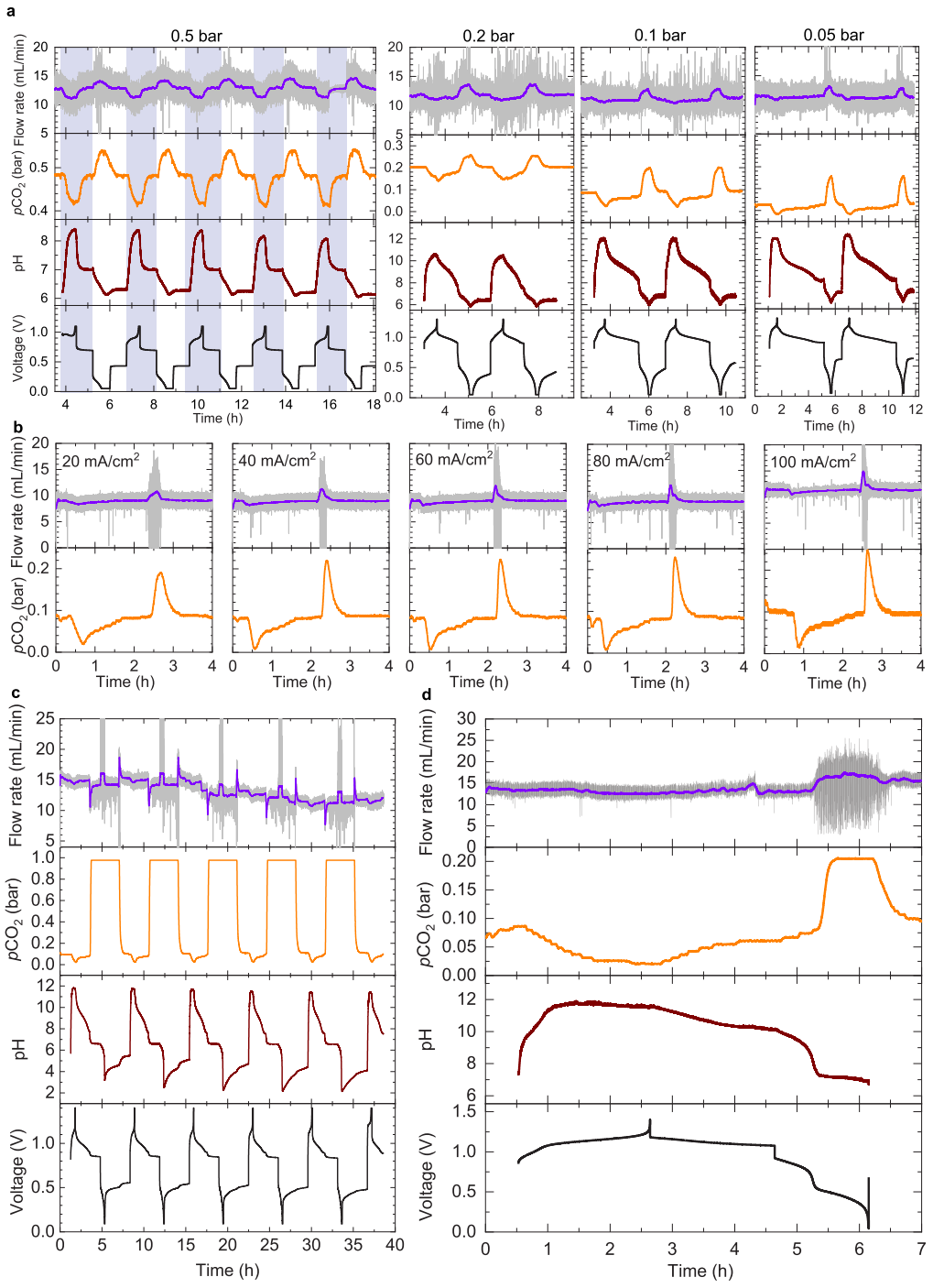

Figure 4. 1,5-BTMAPAQ electrochemical CO_2 capture capability in CO_2−N_2 mixtures. (a) CO_2 capture and release cycling at 20 mA/cm^2. The partial pressure of CO_2 is set to ∼0.05, 0.1, 0.2, and 0.5 bar for the experiments, separately. The plots in panel a share the same *Y*-axis titles and units on the far left. Flow cells comprising 10−12 mL of 0.115 M 1,5-BTMAPAQ in 1 M KCl and 40 mL of 0.2 M FcNCl in 1 M KCl were used for the experiments at 0.05, 0.1, and 0.2 bar. A flow cell comprising 10 mL of 0.115 M 1,5-BTMAPAQ in 1 M KCl and 40 mL of 0.2 M BTMAPFc (bis((3-trimethylammonio)propyl)ferrocene dichloride)[47] in 1 M KCl was used for the experiment at 0.5 bar. (b) Plots presenting the downstream CO_2 partial pressure and the downstream total gas flow rates when the electrochemical redox reactions were triggered at 20, 40, 60, 80, and 100 mA/cm^2. A flow cell comprises 10 mL of 0.057 M 1,5-BTMAPAQ in 1 M KCl and 40 mL of 0.1 M FcNCl in 1 M KCl. (c) CO_2 capture and release cycling where the capture occurred at an inlet CO_2 partial pressure of 0.1 bar and the release occurred at an inlet CO_2 partial pressure of 1 bar. A flow cell comprises 12 mL of 0.115 M 1,5-BTMAPAQ in 1 M KCl and 40 mL of 0.2 M FcNCl in 1 M KCl at 20 mA/cm^2. (d) CO_2 capture and release at an inlet CO_2 partial pressure of 0.1 bar in a flow cell comprising 10 mL of 0.4 M 1,5-BTMAPAQ DI water and 30 mL of 0.9 M FcNCl in DI water at 20 mA/cm^2. Plots present current density, voltage, pH, downstream CO_2 partial pressure, and the downstream total gas flow rate of the 1,5-BTMAPAQ electrolyte. The initial gas flow rate is set to 11.76 mL/min.

BTMAPAQ in their corresponding three states (Figures S1, S3).

To examine the CO_2 capture capability of BTMAPAQs, we first conducted chemically induced CO_2 capture from pure,

https://doi.org/10.1021/acsenergylett.4c01235
ACS Energy Lett. 2024, 9, 3526−3535

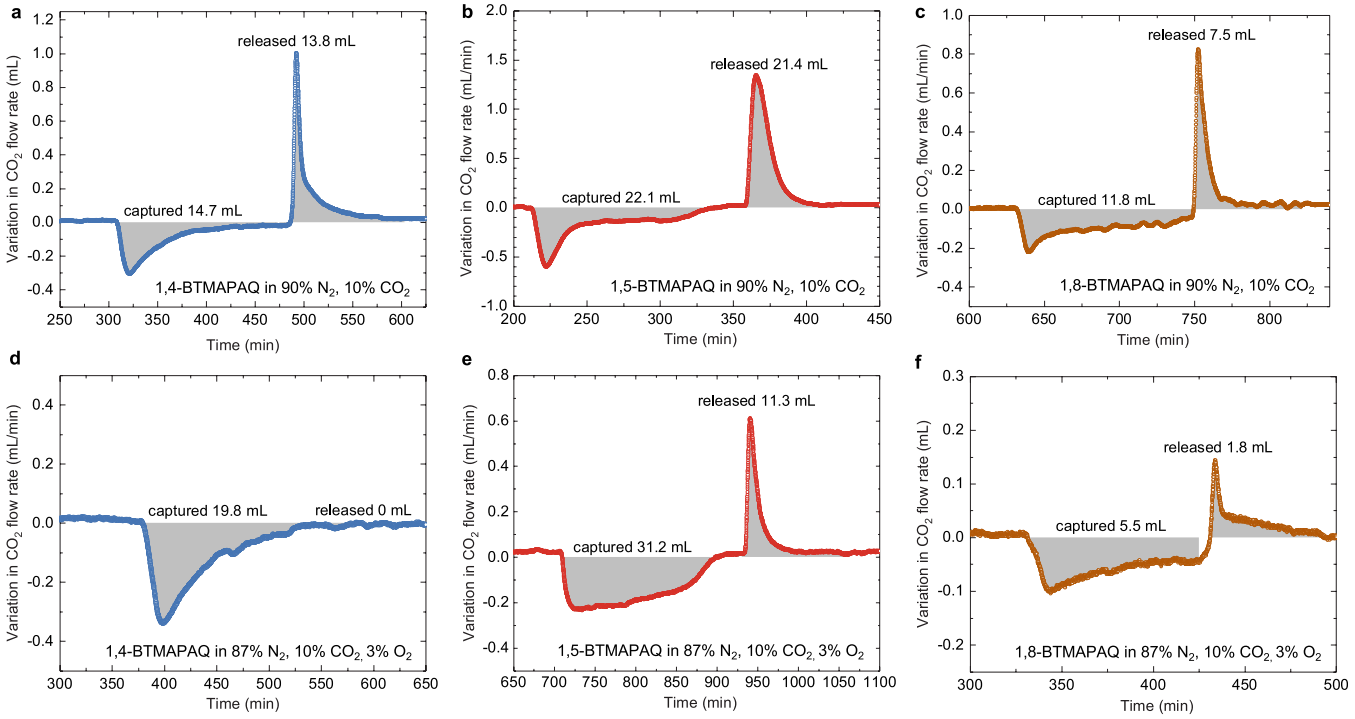

Figure 5. CO_2 capture and release of 1,4-, 1,5-, and 1,8-BTMAPAQs with and without O_2. Calculated volumes of captured and released CO_2 by (a) 1,4-, (b) 1,5-, and (c) 1,8-BTMAPAQs in a feed gas stream of 90% N_2 and 10% CO_2 at 1.0 bar. Calculated volumes of captured and released CO_2 by (d) 1,4-, (e) 1,5-, and (f) 1,8-BTMAPAQs in a feed gas stream of 87% N_2, 10% CO_2, and 3% O_2 (simulated flue gas) at 1.0 bar. 5 mL of 0.1 M 1,4- and 1,5-BTMAPAQs and 1 M KCl solutions were paired with 40 mL of 0.1 M FcNCl and 1 M KCl solution. 5 mL of 0.1 M 1,8-BTMAPAQ and 1 M TBACl solution was paired with 40 mL of 0.1 M FcNCl and 1 M TBACl solution. The BTMAPAQs were electrochemically reduced and oxidized at 40 mA/cm^2, followed by potential holds to complete the reactions. The theoretical CO_2 capture and release capacity for the BTMAPAQ electrolytes is 22.4 mL. Electrochemical reduction/oxidation was followed by a rest time that was adjusted to approach the maximum CO_2 capture/release capacity while minimizing the O_2-induced side reactions. The durations of CO_2 capture/release for 1,4-BTMPAQ are 175/125 min without O_2 and 170/100 min in the simulated gas, respectively. The durations of CO_2 capture/release for 1,5-BTMPAQ are 145/80 min without O_2 and 226/160 min in the simulated gas, respectively. The durations of CO_2 capture/release for 1,8-BTMPAQ are 120/90 min without O_2 and 100/70 min in the simulated gas, respectively. The addition of 1 M TBACl to 0.1 M 1,8-BTMAPAQ increased the viscosity of the solution, slowing the dissolution of CO_2 and O_2 from gas phase to liquid phase.

flowing CO_2, release into N_2, and sequestration as $BaCO_3(s)$, from which we validated the CO_2 capture capacity of 2 CO_2 per quinone (Figure S6). Subsequently, we investigated the electrochemically induced CO_2 capture performance of 1,5-BTMAPAQ at 0.5 bar of CO_2 and 0.5 bar of N_2. (Figure 4a). The electrochemical reduction and oxidation were accompanied by CO_2 capture and release, which were reflected by the periodic oscillation of downstream CO_2 partial pressure and downstream gas flow rate as well as the pH-swing of 1,5-BTMAPAQ electrolyte. A 45 min interval between reduction and oxidation was chosen as the minimum rest time to complete the gas−liquid reaction, which is the rate-limiting step (Figure S7). Integrating the downstream gas flow rate change during the CO_2 release indicates that the measured volume of released CO_2 is almost the same as the theoretical value (Figure S8), suggesting that each 1,5-BTMAPAQ can capture and release two CO_2 molecules. Through analyzing the round-trip voltage efficiency and Coulombic efficiency over five cycles of the electrochemical reduction and oxidation, we found the energetic cost ranges from 65 to 80 kJ/mol CO_2 at 20 mA/cm^2 at a fixed inlet CO_2 partial pressure of 0.5 bar. The close correspondence between the Coulombic efficiency and the CO_2 release/capture efficiency in Figure S8e, defined as the ratio of the amount of CO_2 released to the amount captured in the immediately preceding half-cycle, indicates that CO_2 capture/release is triggered by the electrochemical reactions and mirrored by Coulombic efficiencies.

In real applications, the partial pressure of CO_2 in feed gas varies over a broad range; hence we performed a series of tests in feed gas with varied partial pressure of CO_2 at 0.05, 0.1, 0.2, and 0.5 bar. To increase the CO_2 capture capacity, we adjusted the corresponding rest time intervals as 210, 105, 52, and 45 min, respectively (Figure 4a, Figure S9). During the electrochemical reduction of 1,5-BTMAPAQ, the pH range went from wide to narrow while the CO_2 partial pressure was adjusted from 0.05 to 0.5 bar. For instance, the pH swung from near neutral to ∼12 at 0.05 bar CO_2, but to only ∼9 at 0.5 bar CO_2. According to Henry's law, a higher partial pressure of CO_2 can lead to a higher CO_2 solubility in solution, thus enabling the prompt buffering of pH increase induced by electrochemical reduction. Despite the variation in CO_2 partial pressure, two CO_2 molecules were captured by one 1,5-BTMAPAQ with an energetic cost of 48−50 kJ/molCO_2 at 20 mA/cm^2.

One advantage of aqueous flow chemistry is the capability to operate electrochemical reactions at high current densities. Although extremely diluted CO_2 essentially limits the CO_2 capture heterogeneous chemical reaction rate regardless of technology, CO_2 release in our system is coupled with electrochemical oxidation; thus, the CO_2 release rate can be readily accelerated by applying high current densities. We

https://doi.org/10.1021/acsenergylett.4c01235
ACS Energy Lett. 2024, 9, 3526−3535

electrochemically reduced and oxidized 1,5-BTMAPAQ at 20, 40, 60, 80, and 100 mA/cm^2 in the presence of 0.1 bar of CO_2 (Figure 4b, Figure S10). The depression of downstream CO_2 partial pressure and gas flow rate caused by CO_2 capture was almost the same at that at different current densities, indicating that the CO_2 capture reaction rate is limited by mass transport of 0.1 bar of CO_2 rather than by the electrochemical reduction rate, i.e., the applied current density. However, the peaks of the downstream CO_2 partial pressure and gas flow rate caused by the CO_2 release became sharper and narrower with the increase of current density, suggesting that the CO_2 release rate can be accelerated with increased current density, thus shortening the CO_2 release time. It is worth noting that the calculated volumes of released CO_2 reach the theoretical values at different current densities (Figure S10). The midpoint voltage difference between charge and discharge curves increases with current density, which is caused by internal cell resistance, resulting in a broad energetic cost range of 65−140 kJ/molCO_2.

It is important to evaluate the CO_2 capture capacity and energetic cost when a system is used to capture CO_2 from a dilute source and release it into pure CO_2. Hence, we performed our experiment using 1,5-BTMAPAQ with a 0.1 bar inlet CO_2 and 1.0 bar pure CO_2 exit stream (Figure 4c). The volume of released CO_2 approaches the theoretical value over five cycles (Figure S12). The energetic cost and Coulombic efficiency are either comparable to or slightly higher than those measured under previous conditions (Figures S9−S11).

A concentrated quinone flow system comprising 0.4 M 1,5-BTMAPAQ was set up to demonstrate a high volumetric CO_2 capture capacity (Figure 4d). Because of the low pK_a values (<13) of 1,5-BTMAPH$_2$AQ (Figure 3b), the pH-swing for 0.4 M 1,5-BTMAPAQ is the same as that for 0.1 M 1,5-BTMAPAQ, further supporting our interpretation of the results as the formation of $Q(CO_2)_2^{2-}$. Although the increased concentration of 1,5-BTMAPAQ took a longer time to complete the capture, it still reached the theoretical capacity at an energetic cost of 90 kJ/molCO_2.

In real applications, CO_2 always coexists with O_2 at varying partial pressures, depending on the CO_2 sources. It has been reported that reduced quinones are susceptible to O_2,[23,48,49] which can reversibly chemically oxidize the reduced quinones to their oxidized states. These reduced quinones are the species of interest for binding of CO_2. Hence, we investigated the oxygen sensitivity of the reduced quinones, including H_2Q, HQ^-, Q^{2-}, $HQ(CO_2)^-$, and $Q(CO_2)_2^{2-}$, as capture will become practical only if the reduced quinones become oxidized by O_2 sufficiently slowly in an atmosphere with a relatively high O_2 partial pressure.

The reduced quinones are oxygen-sensitive because their oxidation potentials are much lower than the O_2 reduction potential. In contrast, the oxidation potentials of $Q(CO_2)_2^{2-}$ can positively shift by at least 500 mV compared to those of the reduced quinones (Figure 3a), approaching the reduction potential of O_2 (Figure 3b) and possibly making $Q(CO_2)_2^{2-}$ more O_2-tolerant. Through tracking the ^{1}H NMR of the reduced quinones with and without captured CO_2 during air exposure (Figures S14−S19), we observed that the reduced quinones gradually converted to the oxidized forms over days with different conversion rates. After operating BTMAPAQ flow cells in atmospheres with fixed CO_2 partial pressure but varied O_2 partial pressure (Table S2), we analyzed their Coulombic efficiency to compare the oxygen sensitivity of BTMAPAQ isomers. We also performed chemically induced CO_2 capture, release, and sequestration with air exposure (Figure S20) and found that 1.7 equiv of CO_2 was released when the solution with captured CO_2 was vigorously stirred in air for 15 min. Detailed information is reported in the "Oxygen sensitivity" section of the Supporting Information. Those measurements inspired us to further evaluate BTMAPAQs-based electrochemical CO_2 capture from simulated flue gases with an upgraded system setup (Figures S21−S23). By integrating the peak area of the CO_2 flow rate deviation over CO_2 capture and release cycles (Figure 5), we evaluated the CO_2 capture and release volumes from 1,4-, 1,5-, and 1,8-BTMAPAQs in the absence and presence of O_2. When 1,4- and 1,5-BTMAPAQ were exposed to 1.0 bar feed gas composed of 10% CO_2 and 90% N_2, the CO_2 release/capture volume ratio is close to 1 (Figure 5a, b), suggesting the reversibility of the CO_2 capture and release. When exposed to 1.0 bar simulated flue gas composed of 3% O_2, 10% CO_2, and 87% N_2, the volumes of released CO_2 greatly decrease, which we attribute to the oxygen-induced side reactions shown in Eqns 10 and 11 in Table 1. Compared to the CO_2 capture volumes from 1,4- and 1,5-BTMAPAQs in the absence of O_2, their CO_2 capture volumes in the presence of O_2 become significantly larger, which we attribute to additional CO_2 irreversibly trapped by the hydroxide ions converted from oxygen (Eqns 7, 8, 10, and 11 in Table 1). The superior oxygen tolerance shown by 1,5-BTMAPAQ might be due to its net zero dipole moment and the overall nonpolar structure. Polar molecules tend to have higher reactivity,[50] which may explain the inferior oxygen tolerance shown by 1,4- and 1,8-BTMAPAQs. The CO_2 capture volumes from 1,8-BTMAPAQ are much smaller than those from 1,4- and 1,5-BTMAPAQ, which we tentatively attribute to the increased electrolyte viscosity caused by the addition of 1 M TBA$^+$, which slows the dissolution of CO_2 to the electrolyte, lowering the capture capacity.

Among the three BTMAPAQ isomers, 1,5-BTMAPAQ shows the highest CO_2 capture capacity of 21.4 mL in the absence of O_2, which is close to the theoretical value of 22.4 mL, assuming that one 1,5-BTMAPAQ captures two CO_2 molecules. Under 3% O_2 exposure for 226 min during CO_2 capture for 160 min during the release, 1,5-BTMAPAQ still released 11.3 mL of CO_2, which is ∼50% of the theoretical

Table 1. Electrochemical and Chemical Reactions during CO_2 Capture and Release When Oxygen Is Involved[a]

Stage 1	Electrochemical reduction	Eqn. 1	$AQ + 2e^- \rightarrow AQ^{2-}$
		Eqn. 2	$AQ + 2e^- + 2H_2O \rightarrow H_2AQ + 2OH^-$
		Eqn. 3	$AQ + 2e^- + H_2O \rightarrow HAQ^- + OH^-$
Stage 2	Electrochemically induced CO_2 capture	Eqn. 4	$AQ^{2-} + CO_2 \rightarrow AQ(CO_2)_2^{2-}$
		Eqn. 5	$HAQ^- + CO_2 \rightarrow HAQ(CO_2)^-$
		Eqn. 6	$OH^- + CO_2 \rightarrow HCO_3^-$
	O_2-involved chemical reactions lead to irreversible capture and escape of CO_2	Eqn. 7	$AQ^{2-} + H_2O + 1/2O_2 \rightarrow AQ + 2OH^-$
		Eqn. 8	$HAQ^- + 1/2O_2 \rightarrow AQ + OH^-$
		Eqn. 9	$H_2AQ + 1/2O_2 \rightarrow AQ + H_2O$
		Eqn. 10	$HAQ(CO_2)^- + 1/2O_2 \rightarrow AQ + OH^- + CO_2$
		Eqn. 11	$AQ(CO_2)_2^{2-} + H_2O + 1/2O_2 \rightarrow AQ + 2OH^- + 2CO_2$
Stage 3	Electrochemically induced CO_2 release	Eqn. 12	$AQ(CO_2)_2^{2-} - 2e^- \rightarrow AQ + 2CO_2$
		Eqn. 13	$H_2AQ - 2e^- + 2HCO_3^- \rightarrow AQ + 2H_2O + 2CO_2$
		Eqn. 14	$HAQ(CO_2)^- - 2e^- + HCO_3^- \rightarrow AQ + H_2O + 2CO_2$

[a]The hydroxide ions produced from Eqns 7 and 8 can irreversibly capture CO_2 via Eqn 6. The captured CO_2 can escape due to the chemical oxidation shown in Eqns 10 and 11.

https://doi.org/10.1021/acsenergylett.4c01235
ACS Energy Lett. 2024, 9, 3526−3535

capacity. It is worth noting that the CO_2 capture/release capacity can be further improved by optimizing the CO_2 capture time duration, as with decreased exposure time there should be fewer O_2-induced side reactions and more captured CO_2 will be released. However, if the CO_2 capture duration is too short, both captured and released CO_2 volumes will become small, lowering the faradic efficiency, defined in this context as the ratio of the amount of CO_2 reversibly captured and released to the theoretical capacity. Thus, a trade-off is apparent between the CO_2 release/capture volume ratio and the faradic efficiency. Nevertheless, the O_2 resistance and CO_2 capture capability shown by 1,5-BTMAPAQ in Figure 5e demonstrate that reduced quinones are not necessarily too oxygen-sensitive to be useful for CO_2 capture. The BTMAPAQ-based electrochemical CO_2 capture−release behavior in a simulated flue gas atmosphere over multiple cycles (Figures S24−S27) illustrates that there is still room for improvement of the long-term O_2 tolerance of reduced quinones through judicious molecular design. The distinct O_2 reactivity difference among the isomers implies that a substituent position effect plays a major role in governing the isomers' oxygen tolerance. The substituent positions in the isomers may affect the interaction strength between the positively charged alkylammonium ending groups and the negatively charged phenolate active sites or the organic adducts, further influencing the nucleophilicity-induced CO_2 capture capacity and O_2-induced chemical redox reactions.

More broadly, molecular oxygen tolerance can be improved via molecular engineering with the incorporation of steric and electronic effects, intramolecular interactions, etc. induced by quinone cores or covalently bonded functional groups. The both basicity- and nucleophilicity-based CO_2 capture mechanisms further enlarge the molecular design space, facilitating the discovery of desired molecules.

1. **Steric hindrance** could be introduced to prevent the chemical oxidation between activated molecules and molecular oxygen. Note that the introduction of steric hindrance will make the nucleophilic addition between activated molecules and CO_2 difficult without affecting the basicity of activated molecules, leading to the dominance of pH-swing-based CO_2 capture and release.
2. **Intramolecular hydrogen bonding** can potentially stabilize activated molecules, making it difficult for them to be oxidized by O_2. Apaydin et al.[51] has demonstrated that an activated quinacridone film with captured CO_2 via nucleophilic addition can be stabilized by hydrogen bonds, in which CO_2 can be released only with extra heat or at an applied oxidation potential of 0.7 V vs Fc/Fc^+, which is substantially higher than the oxygen reduction potential (−1.2 V vs Fc/Fc^+).[27] It is thus possible that intramolecular hydrogen bonds can also stabilize activated molecules in solutions.
3. **Elevating the oxidation potentials of activated molecules** above the oxygen reduction potential should make them oxygen-tolerant. Meanwhile, increasing potentials might also decrease the basicity and nucleophilicity of activated molecules, thus making them less capable to capture CO_2 via either mechanism, compromising their CO_2 capture capacity.[48]
4. **Lowering the oxidation potentials of activated molecules** may be a counterintuitive approach to increase the oxygen tolerance of activated molecules. When the Gibbs free energy of the chemical redox reaction between activated molecules and O_2 is too negative and falling into the Marcus inverted region, the reaction rate will decrease as the driving force increases.[52]
5. **Machine learning** is emerging as a powerful approach in materials discovery.[53] It thus has potential to offer valuable guidelines and accelerate the discovery of oxygen-tolerant redox molecules.

Through molecular screening and modification, we developed three water-soluble and anion-exchange membrane compatible bis[3-(trimethylammonio)propyl]anthraquinone (BTMAPAQ) isomers that can be used for electrochemical CO_2 capture. With a series of characterizations including cyclic voltammetry, Pourbaix diagram analysis, ^1H and ^{13}C NMR, electrochemical charge−discharge voltage−capacity profiles, and in situ monitoring of pH, p_{CO2}, and gas flow rate, we showed that aqueous quinone flow chemistry-enabled electrochemical CO_2 capture proceeds via pH-swing and nucleophilicity-swing mechanisms. The latter is more dominant because of the low pK_a values of hydroquinones. 1,5-BTMAPAQ electrolyte can capture and release the theoretical limit of 2 equiv of CO_2 molecules per quinone from 1-bar CO_2−N_2 mixtures for which the CO_2 partial pressure is as low as 0.05 bar, or the applied current density is as high as 100 mA/cm^2, or the organic concentration is as high as 0.4 M, with an energetic cost ranging from 48 to 140 kJ/mol CO_2. When exposed to a simulated flue gas comprising 3% O_2, 10% CO_2, and 87% N_2 at 1.0 bar total pressure for over 4 h, 1,5-BTMAPAQ reversibly captured and released 50% of the theoretical capacity. The distinct position effect on O_2 reactivity exhibited by BTMAPAQ isomers illustrates the opportunity for molecular engineering for further improvement of the molecular properties. This may stimulate the progress of oxygen-tolerant, low-cost, scalable aqueous quinone flow chemistry enabling electrochemical CO_2 capture.

■ ASSOCIATED CONTENT

Data Availability Statement

Data for this article, including cyclic voltammograms, other data files produced by potentiostats, pH readings, gas volumetric flow rates, and partial pressure readings, are available at https://zenodo.org/doi/10.5281/zenodo.11968537.

Supporting Information

The Supporting Information is available free of charge at https://pubs.acs.org/doi/10.1021/acsenergylett.4c01235.

General experimental procedures; solubility of anthraquinones; oxygen sensitivity of reduced anthraquinones; chemical CO_2 capture, release, and sequestration in the absence/presence of O_2; electrochemical CO_2 capture in the absence/presence of O_2 (PDF)

■ AUTHOR INFORMATION

Corresponding Authors

Roy G. Gordon − *Department of Chemistry and Chemical Biology, Harvard University, Cambridge, Massachusetts 02138, United States; John A. Paulson School of Engineering and Applied Sciences, Harvard University, Cambridge, Massachusetts 02138, United States;* orcid.org/0000-0001-5980-268X; Email: gordon@chemistry.harvard.edu

https://doi.org/10.1021/acsenergylett.4c01235
ACS Energy Lett. 2024, 9, 3526−3535

Michael J. Aziz − *John A. Paulson School of Engineering and Applied Sciences, Harvard University, Cambridge, Massachusetts 02138, United States;* orcid.org/0000-0001-9657-9456; Email: maziz@harvard.edu

Authors

Yan Jing − *Department of Chemistry and Chemical Biology, Harvard University, Cambridge, Massachusetts 02138, United States; John A. Paulson School of Engineering and Applied Sciences, Harvard University, Cambridge, Massachusetts 02138, United States;* Present Address: National University of Singapore, 117575, Singapore; orcid.org/0000-0002-5669-4609

Kiana Amini − *John A. Paulson School of Engineering and Applied Sciences, Harvard University, Cambridge, Massachusetts 02138, United States;* Present Address: University of British Columbia, Vancouver V6T 1Z4, BC, Canada

Dawei Xi − *John A. Paulson School of Engineering and Applied Sciences, Harvard University, Cambridge, Massachusetts 02138, United States;* orcid.org/0000-0002-5412-3474

Shijian Jin − *John A. Paulson School of Engineering and Applied Sciences, Harvard University, Cambridge, Massachusetts 02138, United States;* Present Address: X, the moonshot factory, Mountain View, California 94043, United States

Abdulrahman M. Alfaraidi − *John A. Paulson School of Engineering and Applied Sciences, Harvard University, Cambridge, Massachusetts 02138, United States*

Emily F. Kerr − *Department of Chemistry and Chemical Biology, Harvard University, Cambridge, Massachusetts 02138, United States;* Present Address: Xavier University, Cincinnati, Ohio 45207, United States

Complete contact information is available at: https://pubs.acs.org/10.1021/acsenergylett.4c01235

Author Contributions

[▽]Y.J. and K.A. contributed equally to this work.

Notes

The authors declare no competing financial interest.

■ ACKNOWLEDGMENTS

Research at Harvard was supported by the Harvard Climate Change Solutions Fund. K.A. was supported in part by U.S. DOE award DE-AC05-76RL01830 through PNNL subcontract 654799 and in part through the Natural Sciences and Engineering Research Council of Canada (NSERC) Postdoctoral Fellowship (PDF) program [application number PDF-557232-2021]. We acknowledge Alexander Forse from Univ. of Cambridge for useful discussions. We thank Prof. Theodore A. Betley, Dr. Thomas Cochard, Andrew Bergman, Toly Rinberg, Eric M. Fell, Thomas Y. George, Maia Alberts, Michael Emanuel, Dr. Tatsuhiro Tsukamoto, and Dr. Jinxu Gao for useful discussions.

■ REFERENCES

(1) House, K. Z.; Baclig, A. C.; Ranjan, M.; van Nierop, E. A.; Wilcox, J.; Herzog, H. J. Economic and Energetic Analysis of Capturing CO2 from Ambient Air. *Proc. Natl. Acad. Sci. U.S.A.* **2011**, *108*, 20428.

(2) Zito, A. M.; Clarke, L. E.; Barlow, J. M.; Bim, D.; Zhang, Z.; Ripley, K. M.; Li, C. J.; Kummeth, A.; Leonard, M. E.; Alexandrova, A. N.; Brushett, F. R.; Yang, J. Y. Electrochemical Carbon Dioxide Capture and Concentration. *Chem. Rev.* **2023**, *123*, 8069.

(3) Diederichsen, K. M.; Sharifian, R.; Kang, J. S.; Liu, Y.; Kim, S.; Gallant, B. M.; Vermaas, D.; Hatton, T. A. Electrochemical Methods for Carbon Dioxide Separations. *Nature Reviews Methods Primers* **2022**, *2*, 68.

(4) Rahimi, M.; Khurram, A.; Hatton, T. A.; Gallant, B. Electrochemical Carbon Capture Processes for Mitigation of CO_2 Emissions. *Chem. Soc. Rev.* **2022**, *51*, 8676.

(5) Barlow, J. M.; Clarke, L. E.; Zhang, Z.; Bim, D.; Ripley, K. M.; Zito, A.; Brushett, F. R.; Alexandrova, A. N.; Yang, J. Y. Molecular Design of Redox Carriers for Electrochemical CO_2 Capture and Concentration. *Chem. Soc. Rev.* **2022**, *51*, 8415.

(6) O'Brien, P. J. Molecular Mechanisms of Quinone Cytotoxicity. *Chem.-Biol. Interactions* **1991**, *80*, 41.

(7) Nowicka, B.; Kruk, J. Occurrence, Biosynthesis and Function of Isoprenoid Quinones. *Biochim. Biophys. Acta* **2010**, *1797*, 1587.

(8) Dulo, B.; Phan, K.; Githaiga, J.; Raes, K.; De Meester, S. Natural Quinone Dyes: A Review on Structure, Extraction Techniques, Analysis and Application Potential. *Waste and Biomass Valorization* **2021**, *12*, 6339.

(9) Campos-Martin, J. M.; Blanco-Brieva, G.; Fierro, J. L. Hydrogen Peroxide Synthesis: An Outlook Beyond the Anthraquinone Process. *Angew. Chem., Int. Ed. Engl.* **2006**, *45*, 6962.

(10) Jing, Y.; Gordon, R.G.; Aziz, M. J. *Aqueous Organic Flow Batteries*; Wiley-VCH: Weinheim, 2023; Vol. 3.

(11) Mizen, M. B.; Wrighton, M. S. Reductive Addition of CO_2 to 9,10-Phenanthrenequinone. *J. Electrochem. Soc.* **1989**, *136*, 941.

(12) Scovazzo, P.; Poshusta, J.; DuBois, D.; Koval, C.; Noble, R. Electrochemical Separation and Concentration of 1% CO_2 from Nitrogen. *J. Electrochem. Soc.* **2003**, *150*, D91.

(13) Quan, M.; Sanchez, D.; Wasylkiw, M. F.; Smith, D. K. Voltammetry of Quinones in Unbuffered Aqueous Solution: Reassessing the Roles of Proton Transfer and Hydrogen Bonding in the Aqueous Electrochemistry of Quinones. *J. Am. Chem. Soc.* **2007**, *129*, 12847.

(14) Watkins, J. D.; Siefert, N. S.; Zhou, X.; Myers, C. R.; Kitchin, J. R.; Hopkinson, D. P.; Nulwala, H. B. Redox-Mediated Separation of Carbon Dioxide from Flue Gas. *Energy Fuels* **2015**, *29*, 7508.

(15) Huang, C. L.; Liu, C. J.; Wu, K. J.; Yue, H. R.; Tang, S. Y.; Lu, H. F.; Liang, B. CO_2 Capture from Flue Gas Using an Electrochemically Reversible Hydroquinone/Quinone Solution. *Energy Fuels* **2019**, *33*, 3380.

(16) Jin, S.; Wu, M.; Gordon, R. G.; Aziz, M. J.; Kwabi, D. G. pH Swing Cycle for CO_2 Capture Electrochemically Driven through Proton-Coupled Electron Transfer. *Energy Environ. Sci.* **2020**, *13*, 3706.

(17) Xie, H.; Jiang, W.; Liu, T.; Wu, Y.; Wang, Y.; Chen, B.; Niu, D.; Liang, B. Low-Energy Electrochemical Carbon Dioxide Capture Based on a Biological Redox Proton Carrier. *Cell Reports Physical Science* **2020**, *1*, 100046.

(18) Gurkan, B.; Simeon, F.; Hatton, T. A. Quinone Reduction in Ionic Liquids for Electrochemical CO_2 Separation. *ACS Sustainable Chem. Eng.* **2015**, *3*, 1394.

(19) Wielend, D.; Apaydin, D. H.; Sariciftci, N. S. Anthraquinone Thin-Film Electrodes for Reversible CO_2 Capture and Release. *Journal of Materials Chemistry A* **2018**, *6*, 15095.

(20) Voskian, S.; Hatton, T. A. Faradaic Electro-Swing Reactive Adsorption for CO_2 Capture. *Energy Environ. Sci.* **2019**, *12*, 3530.

(21) Liu, Y.; Ye, H. Z.; Diederichsen, K. M.; Van Voorhis, T.; Hatton, T. A. Electrochemically Mediated Carbon Dioxide Separation with Quinone Chemistry in Salt-Concentrated Aqueous Media. *Nat. Commun.* **2020**, *11*, 2278.

(22) Diederichsen, K. M.; Liu, Y.; Ozbek, N.; Seo, H.; Hatton, T. A. Toward Solvent-Free Continuous-Flow Electrochemically Mediated Carbon Capture with High-Concentration Liquid Quinone Chemistry. *Joule* **2022**, *6*, 221.

(23) Barlow, J. M.; Yang, J. Y. Oxygen-Stable Electrochemical CO_2 Capture and Concentration with Quinones Using Alcohol Additives. *J. Am. Chem. Soc.* **2022**, *144*, 14161.
(24) Eisaman, M. D.; Alvarado, L.; Larner, D.; Wang, P.; Garg, B.; Littau, K. A. CO_2 separation Using Bipolar Membrane Electrodialysis. *Energy Environ. Sci.* **2011**, *4*, 1319.
(25) Eisaman, M.D.; Alvarado, L.; Larner, D.; Wang, P.; Littau, K.A. CO_2 Desorption Using High-Pressure Bipolar Membrane Electrodialysis. *Energy Environ. Sci.* **2011**, *4*, 4031.
(26) Rahimi, M.; Catalini, G.; Puccini, M.; Hatton, T. A. Bench-Scale Demonstration of CO_2 Capture with an Electrochemically Driven Proton Concentration Process. *RSC Adv.* **2020**, *10*, 16832.
(27) Li, X.; Zhao, X.; Liu, Y.; Hatton, T. A.; Liu, Y. Redox-Tunable Lewis Bases for Electrochemical Carbon Dioxide Capture. *Nature Energy* **2022**, *7*, 1065.
(28) Jin, S.; Wu, M.; Jing, Y.; Gordon, R. G.; Aziz, M. J. Low Energy Carbon Capture Via Electrochemically Induced pH Swing with Electrochemical Rebalancing. *Nat. Commun.* **2022**, *13*, 2140.
(29) Seo, H.; Rahimi, M.; Hatton, T. A. Electrochemical Carbon Dioxide Capture and Release with a Redox-Active Amine. *J. Am. Chem. Soc.* **2022**, *144*, 2164.
(30) Seo, H.; Hatton, T. A. Electrochemical Direct Air Capture of CO_2 Using Neutral Red as Reversible Redox-Active Material. *Nat. Commun.* **2023**, *14*, 313.
(31) Pang, S.; Jin, S.; Yang, F.; Alberts, M.; Li, L.; Xi, D.; Gordon, R. G.; Wang, P.; Aziz, M. J.; Ji, Y. A Phenazine-Based High-Capacity and High-Stability Electrochemical CO_2 Capture Cell with Coupled Electricity Storage. *Nature Energy* **2023**, *8*, 1126.
(32) Luo, L.; Hou, L.; Liu, Y.; Wu, K.; Zhu, Y.; Lu, H.; Liang, B. Regeneration of Na_2Q in an Electrochemical CO_2 Capture System. *Energy Fuels* **2021**, *35*, 12260.
(33) Jin, S.; Jing, Y.; Kwabi, D. G.; Ji, Y.; Tong, L.; De Porcellinis, D.; Goulet, M. A.; Pollack, D. A.; Gordon, R. G.; Aziz, M. J. A Water-Miscible Quinone Flow Battery with High Volumetric Capacity and Energy Density. *ACS Energy Letters* **2019**, *4*, 1342.
(34) Ji, Y.; Goulet, M.-A.; Pollack, D. A.; Kwabi, D. G.; Jin, S.; De Porcellinis, D.; Kerr, E. F.; Gordon, R. G.; Aziz, M. J. A Phosphonate-Functionalized Quinone Redox Flow Battery at near-Neutral pH with Record Capacity Retention Rate. *Adv. Energy Mater.* **2019**, *9*, 1900039.
(35) Rahimi, M.; Catalini, G.; Hariharan, S.; Wang, M.; Puccini, M.; Hatton, T. A. Carbon Dioxide Capture Using an Electrochemically Driven Proton Concentration Process. *Cell Reports Physical Science* **2020**, *1*, 100033.
(36) Yan, L.; Bao, J.; Shao, Y.; Wang, W. An Electrochemical Hydrogen-Looping System for Low-Cost CO_2 Capture from Seawater. *ACS Energy Letters* **2022**, *7*, 1947.
(37) Huskinson, B. T.; Marshak, M. P.; Suh, C.; Er, S.; Gerhardt, M. R.; Galvin, C. J.; Chen, X.; Aspuru-Guzik, A.; Gordon, R. G.; Aziz, M. J. A Metal-Free Organic-Inorganic Aqueous Flow Battery. *Nature* **2014**, *505*, 195.
(38) Lin, K.; Chen, Q.; Gerhardt, M. R.; Tong, L.; Kim, S. B.; Eisenach, L.; Valle, A. W.; Hardee, D.; Gordon, R. G.; Aziz, M. J.; Marshak, M. P. Alkaline Quinone Flow Battery. *Science* **2015**, *349*, 1529.
(39) Jing, Y.; Zhao, E. W.; Goulet, M. A.; Bahari, M.; Fell, E. M.; Jin, S.; Davoodi, A.; Jonsson, E.; Wu, M.; Grey, C. P.; Gordon, R. G.; Aziz, M. J. In Situ Electrochemical Recomposition of Decomposed Redox-Active Species in Aqueous Organic Flow Batteries. *Nat. Chem.* **2022**, *14*, 1103.
(40) Hu, B.; Luo, J.; Hu, M.; Yuan, B.; Liu, T. L. A pH-Neutral, Metal-Free Aqueous Organic Redox Flow Battery Employing an Ammonium Anthraquinone Anolyte. *Angew. Chem., Int. Ed.* **2019**, *58*, 16629.
(41) Kerr, E. F.; Tang, Z.; George, T. Y.; Jin, S.; Fell, E. M.; Amini, K.; Jing, Y.; Wu, M.; Gordon, R. G.; Aziz, M. J. High Energy Density Aqueous Flow Battery Utilizing Extremely Stable, Branching-Induced High-Solubility Anthraquinone near Neutral pH. *ACS Energy Letters* **2023**, *8*, 600.
(42) Marcus, Y. Tetraalkylammonium Ions in Aqueous and Non-Aqueous Solutions. *J. Solution Chem.* **2008**, *37*, 1071.
(43) Wang, J.; Hou, T. Recent Advances on Aqueous Solubility Prediction. *Combinatorial Chemistry & High Throughput Screening* **2011**, *14*, 328.
(44) Zhu, Y.; Li, Y.; Qian, Y.; Zhang, L.; Ye, J.; Zhang, X.; Zhao, Y. Anthraquinone-Based Anode Material for Aqueous Redox Flow Batteries Operating in Nondemanding Atmosphere. *J. Power Sources* **2021**, *501*, 229984.
(45) Seravalli, J.; Ragsdale, S. W. 13C NMR Characterization of an Exchange Reaction between CO and CO_2 Catalyzed by Carbon Monoxide Dehydrogenase. *Biochemistry* **2008**, *47*, 6770.
(46) Hu, B.; DeBruler, C.; Rhodes, Z.; Liu, T. L. Long-Cycling Aqueous Organic Redox Flow Battery (AORFB) toward Sustainable and Safe Energy Storage. *J. Am. Chem. Soc.* **2017**, *139*, 1207.
(47) Beh, E. S.; De Porcellinis, D.; Gracia, R. L.; Xia, K. T.; Gordon, R. G.; Aziz, M. J. A Neutral pH Aqueous Organic-Organometallic Redox Flow Battery with Extremely High Capacity Retention. *ACS Energy Letters* **2017**, *2*, 639.
(48) Bui, A. T.; Hartley, N. A.; Thom, A. J. W.; Forse, A. C. Trade-Off between Redox Potential and the Strength of Electrochemical CO_2 Capture in Quinones. *J. Phys. Chem. C Nanomater. Interfaces* **2022**, *126*, 14163.
(49) Zito, A. M.; Bím, D.; Vargas, S.; Alexandrova, A. N.; Yang, J. Y. Computational and Experimental Design of Quinones for Electrochemical CO_2 Capture and Concentration. *ACS Sustainable Chem. Eng.* **2022**, *10*, 11387.
(50) Arnaut, L. Pharmacokinetics. *Chemical Kinetics*; Elsevier, 2021; p 441. DOI: 10.1016/b978-0-444-64039-0.00013-3.
(51) Apaydin, D. H.; Glowacki, E. D.; Portenkirchner, E.; Sariciftci, N. S. Direct Electrochemical Capture and Release of Carbon Dioxide Using an Industrial Organic Pigment: Quinacridone. *Angew. Chem., Int. Ed. Engl.* **2014**, *53*, 6819.
(52) Miller, J. R.; Calcaterra, L. T.; Closs, G. L. Intramolecular Long-Distance Electron Transfer in Radical Anions. The Effects of Free Energy and Solvent on Teh Reaction Rates. *J. Am. Chem. Soc.* **1984**, *106*, 3047.
(53) Rahimi, M.; Moosavi, S. M.; Smit, B.; Hatton, T. A. Toward Smart Carbon Capture with Machine Learning. *Cell Reports Physical Science* **2021**, *2*, 100396.

https://doi.org/10.1021/acsenergylett.4c01235
ACS Energy Lett. 2024, 9, 3526−3535

Supplementary information

Electrochemically induced CO_2 capture enabled by aqueous quinone flow chemistry

Yan Jing,[1,2,3] Kiana Amini,[2,3] Dawei Xi,[2] Shijian Jin,[2] Abdulrahman M. Alfaraidi,[2] Emily F. Kerr,[1] Roy G. Gordon,[1,2*] Michael J. Aziz[2*]

1. Department of Chemistry and Chemical Biology, Harvard University, Cambridge, Massachusetts 02138, United States
2. John A. Paulson School of Engineering and Applied Sciences, Harvard University, Cambridge, Massachusetts 02138, United States
3. These authors contributed equally to this work.

* E-mail: gordon@chemistry.harvard.edu; maziz@harvard.edu.

Table of Contents

General experimental procedures

To a 1 L of flame dried Schlenk flask, 40 mmol of dihydroxyanthraquinone, 88 mmol of anhydrous K_2CO_3, and 9.5 mmol of KI were suspended in 160 mL of anhydrous DMF. After being stirred under nitrogen for 20 mins, 88 mmol of 3-bromopropyl trimethylammonium bromide was added to the dark suspension. The dark suspension was sealed to prevent ambient moisture, then was vigorously stirred at 100 ˚C for 16 hours to afford a brownish slurry.

After being cooling down, the slurry was added with 150 mL of ethyl acetate, stirred at room temperature for 30 mins, then filtered to collect the brown cake. The washing procedure was repeated for few times until the filtrate became colorless. The cake was dissolved into methanol, and the solution was filtered to remove insoluble inorganic salts. The filtrate was condensed under vacuo to remove methanol and collect the dark red solid, which was then redissolved in deionized water.

The aqueous quinone solution was then transferred to an anion-exchange resin column prepared in advance to replace bromide with chloride ions. The dark red (bright yellow depending on the concentration) solution was condensed under vacuo to remove water and collect the red solid.

The red solid was re-dissolved in methanol to get the saturated solution, which was then drop-wise added to 200 mL of ethyl acetate and afford precipitates. The precipitates were collected by filtration to get final orange to yellow cakes. The yields range from 85% to 95%.

Among the four BTMAPAQ isomers, the synthesis of 1,8-BTMAPAQ was reported elsewhere.[1]

The syntheses of AQ-1,8-3E-OH and 2,6-D2PEAQ were followed with our previous work without further modification.[2,3]

Structural characterization

^{1}H, ^{13}C NMR spectra were recorded on Varian INOVA 500 spectrometers at 500 MHz. Aliquots were prepared in deuterated water (D_2O), corresponding NMR spectra were recorded in D_2O with the residual H_2O (δ 4.79 ppm for ^{1}H NMR).

Electrochemical characterizations

Glassy carbon was used as the working electrode for all three-electrode cyclic voltammetry measurements with a 5 mm diameter glassy carbon working electrode, an Ag/AgCl reference electrode (BASi, pre-soaked in 3 M NaCl solution), and a graphite counter electrode. All cyclic voltammetry, linear sweep voltammetry, and chronoamperometry measurements were conducted on Gamry Instruments and CHI Instrument electrochemical analysers.

Flow cell assembly

Flow cell experiments were constructed with cell hardware from Fuel Cell Tech (Albuquerque, NM). The flow cell was assembled into a zero-gap flow cell configuration using pyrosealed POCO graphite flow plates with identical interdigitated flow fields. Each electrode was composed of 1 layer of AvCarb HCBA carbon cloth with a 5 cm^2 geometric surface area. Selemion DSV-N was used as the anion exchange membrane. The flow rate was set at 50–70 mL/min. Biologic SP-150e and Gamry Reference 3000 potentiostat was used as our electrochemical workstation. KNF diaphragm pumps were used to circulate electrolytes through the flow fields and electrodes in the cell stack. For some tests, a Cole-Parmer Digital gear pump was used.

Bis((3-trimethylammonio)propyl)ferrocene dichloride (BTMAPFc) and (ferrocenylmethyl)trimethylammonium Chloride (FcNCl) were purchased from TCI-America chemical company. Tetramethyl ammonium chloride, tetrabutylammonium chloride were purchased from Sigma Aldrich. All those chemicals were directly used without further purification.

Electrochemical CO_2 capture and release

Flow cells were charged at constant current, followed by voltage holds until current hits the background current values. Then the flow cells were set in rest mode for certain time to complete carbon capture. The cells were discharged at constant current, followed by a voltage hold. After the voltage hold, the battery was set in rest mode to complete CO_2 release. FS4001 MEMS Mass Flow Sensor, LuminOX O_2 sensor (CM-42990), SprintIR CO_2 sensor (GC-0018) were used in our tests.

A stream of feed gas composed of N_2, CO_2, and O_2 was introduced to the anthraquinone electrolytes and kept flowing constantly with pre-set partial pressure. The total pressure is 1 bar, and the total flow rate is 11.76 mL/min.

The cell testing condition for Fig. 3c is shown below:

During the charge-discharge process, a constant current density of 20 mA/cm^2 was first applied until the voltages approached the pre-set cutoffs. Potential holds were applied at 1.45 V for the charge in pure N_2, 1.5 V for the charge in 90% N_2 and 10% CO_2, and 0.05 V for the discharge until the current density decreased to 1 mA/cm^2.

The cell testing conditions for Fig. 4 are shown below:

Experiments at different current density:

Flow cells were charged using the constant current specified in each plot (20, 40, 60, 80, 100 mA/cm^2). This constant current was applied until the charging voltage reached 1.5 V. Afterward, the voltage was held at this value until the current dropped to 5 mA/cm^2. During discharge, the corresponding constant current (20, 40, 60, 80, 100 mA/cm^2) was applied until the discharge voltage reached 0.05 V. Afterward, the voltage was held at this value until the current dropped to 1 mA/cm^2.

Experiments at different partial pressures:

For partial pressures of 0.05 bar, 0.1 bar, and 0.2 bar, a constant current of 20 mA/cm^2 was applied until the charging voltage reached 1.3 V. Afterward, the voltage was held at this value until the current dropped to 5 mA/cm^2. During discharge, a 20 mA/cm^2 constant current was applied until the discharge voltage reached 0.05 V. Afterward, the voltage was held at this value until the current dropped to 1 mA/cm^2. For the test conducted under a partial pressure of 0.5 bar, the same protocol was used except that the charging voltage was set at 1.1 V instead of 1.3 V. This adjustment was necessary because 1,1'-Bis[3-(trimethylammonio)propyl]ferrocene Dichloride (BTMAPFc) was used instead of ferrocenymetyltrimethylammonium Chloride (FcNCl) as the posolyte electrolyte (counter reaction), requiring a slightly lower charging voltage.

Experiment at 10% – 100% CO_2 purge:

For the tests conducted where the capture occurred in an inlet CO_2 partial pressure of 0.1 bar and release occurred into an inlet CO_2 partial pressure of 1 bar, a constant current of 20 mA/cm² was applied until the charging voltage reached 1.4 V. Afterward, the voltage was held at this value until the current dropped to 5 mA/cm². During discharge, the 20 mA/cm² constant current was applied until the discharge voltage reached 0.1 V. Afterward, the voltage was held at this value until the current dropped to 1 mA/cm².
Experiment at high concentration:
For the tests conducted at the high concentration of 0.4 M, a constant current of 20 mA/cm² was applied until the charging voltage reached 1.4 V. Afterward, the voltage was held at this value until the current dropped to 5 mA/cm². During discharge, the 20 mA/cm² constant current was applied until the discharge voltage reached 0.1 V. Afterward, the voltage was held at this value until the current dropped to 1 mA/cm².

Solubility of anthraquinones in different stages in different supporting salts

Table S1 | Solubility behavior of anthraquinones in different supporting salts.

Compound	Q solubility @ pH 7	0.1 M $Q(CO_2)_2^{2-}$		
		+ 1 M K^+/Na^+	+ 1 M TBA^+	+ 1 M TMA^+
AQDS	0.3	insoluble	insoluble	soluble
AQ-1,8-3E-OH	2.2	insoluble	soluble	insoluble
2,6-D2PEAQ	2.0	insoluble	soluble	insoluble
1,4-BTMAPAQ	1.0	soluble		
1,5-BTMAPAQ	1.3	soluble		
1,8-BTMAPAQ	1.0	insoluble	soluble	
2,6-BTMAPAQ	< 0.1	N/A		

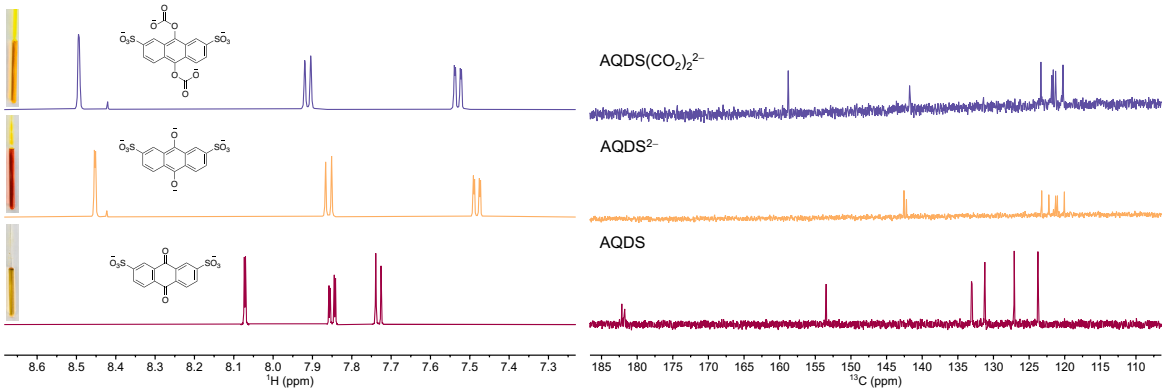

Figure S1 | ^1H and ^{13}C NMR spectra of 0.1 M AQDS, $AQDS^{2-}$, $AQDS(CO_2)_2^{2-}$ 1 M TMACl D_2O solutions. The corresponding color is yellow, red, and bright yellow.

Compatibility issue between bulky alkylammonium cation (TBA^+) and cation-exchange membrane

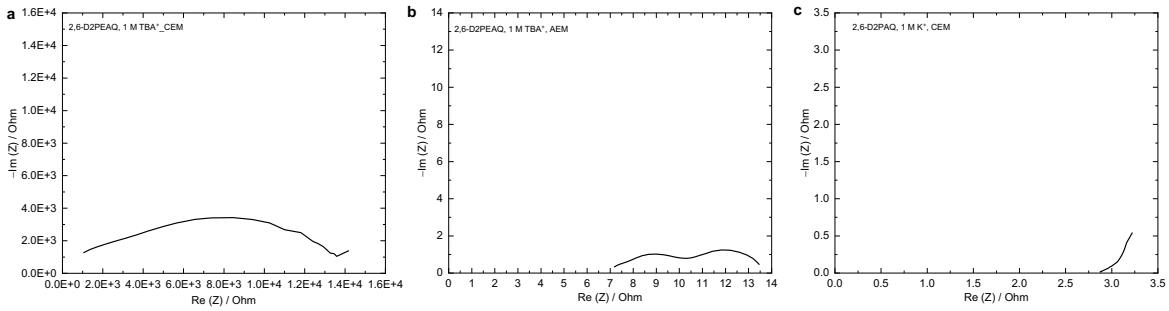

Figure S2 | Electrochemical impedance spectroscopy (EIS) measurement of 2,6-D2PEAQ flow cells. Alternating current area-specific resistance of the cells were determined via high-frequency EIS. (a) 0.1 M 2,6-D2PEAQ, 1 M TBA^+ | 0.1 M $Fe(CN)_6^{3/4-}$, 1 M TBA^+, where a cation-exchange membrane, Nafion 212, was used to separate the electrolytes. (b) 0.1 M 2,6-D2PEAQ, 1 M TBA^+ | 0.1 M $Fe(CN)_6^{3/4-}$, 1 M TBA^+, where an anion-exchange membrane, DSV-N, was used to separate the electrolytes. (c) 0.1 M 2,6-D2PEAQ, 1 M K^+ | 0.1 M $Fe(CN)_6^{3/4-}$, 1 M K^+, where a cation-exchange membrane, Nafion 212 was used to separate the electrolytes. The impedance measurements were conducted at 0% of state of charge. The geographic area of electrode is 5 cm^2.

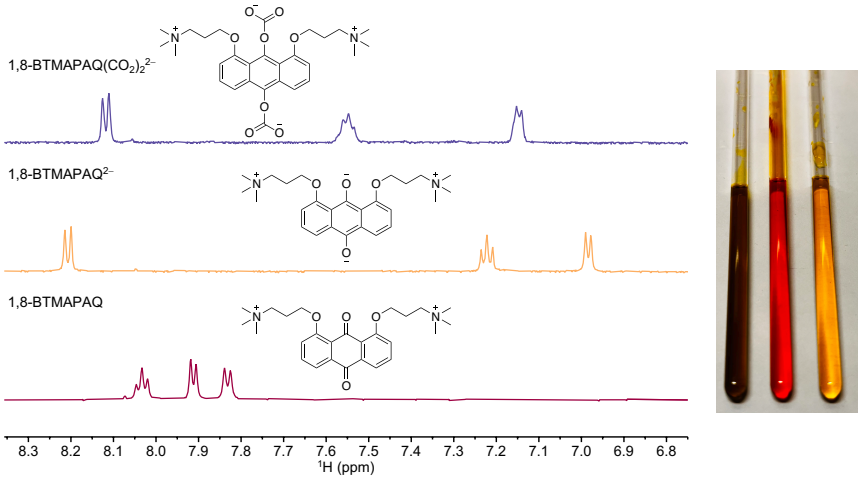

Figure S3 | Stacked ^1H NMR spectra of 1,8-BTMAPAQ in three states. Bottom to top: (1): 0.1 M 1,8-BTMAPAQ in 1 M TBA^+; (2) 0.1 M reduced 1,8-BTMAPAQ in 1 M TBA^+; (3) 0.1 M reduced 1,8-BTMAPAQ with saturated CO_2 in 1 M TBA^+. The corresponding color is brown, red, and bright yellow. We selected 6.7 ppm–8.4 ppm to highlight the chemical shifts in the aromatic region.

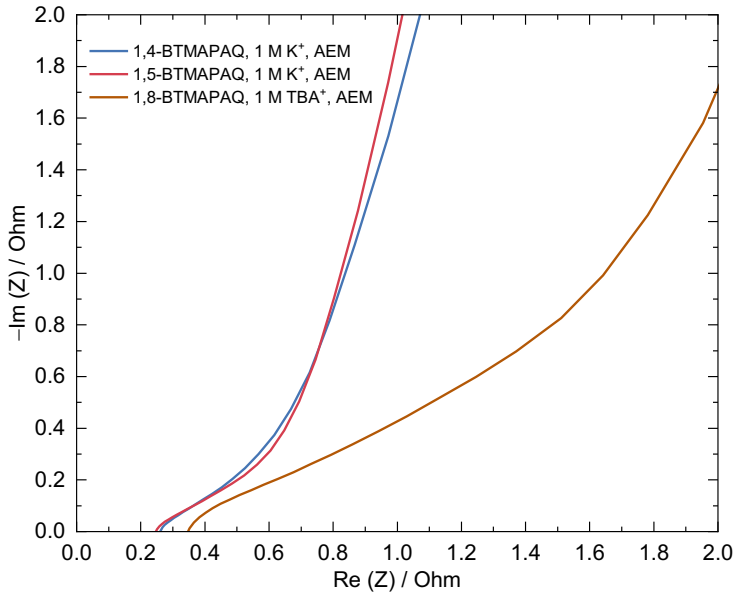

Figure S4 | Electrochemical impedance spectroscopy (EIS) measurement of 0.1 M BTMAPAQ | 0.1 M FeNCl flow cells, where an anion-exchange membrane, DSV-N, was used to separate the electrolytes. The supporting salt of 1,4-, 1,5-BTMAPAQ electrolytes is 1 M KCl, whereas the supporting salt of 0.1 M 1,8-BTMAPAQ electrolyte is 1 M TBACl. The impedance measurements were conducted at 0% of state of charge. The geographic area of electrode is 5 cm^2.

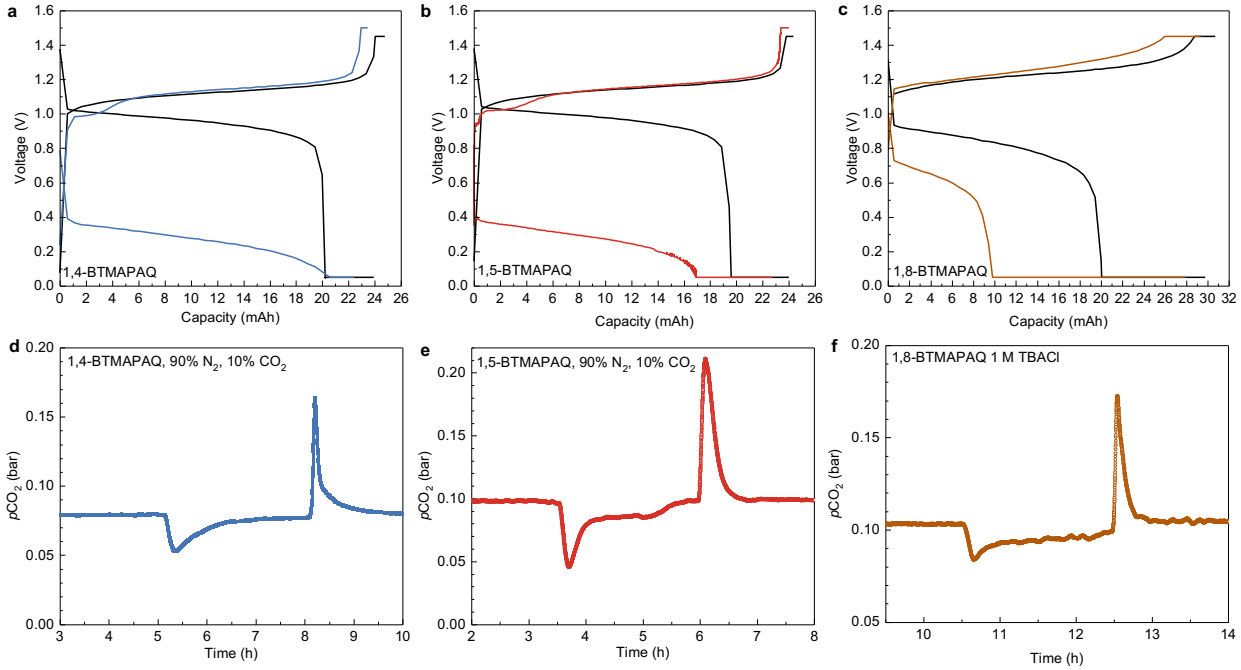

Figure S5 | Voltage profiles and CO_2 partial pressure during the electrochemical reduction and oxidation of BTMAPAQs. Electrolyte composition: 5 mL 0.1 M 1,4-, 1,5-BTMAPAQs, 1 M KCl vs. 40 mL 0.1 M FcNCl, 1 M KCl. 5 mL 0.1 M 1,8-BTMAPAQ, 1 M TBACl vs. 40 mL 0.1 M FcNCl, 1 M TBACl. Constant current (40 mA/cm^2) was followed with potential holds.

Chemical CO_2 capture, release, and sequestration procedure in the absence of O_2

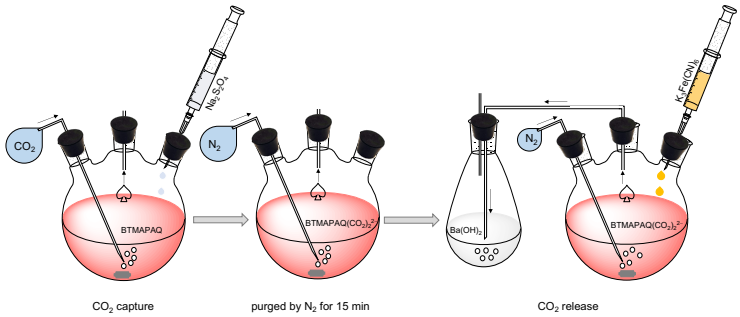

Figure S6 | Chemically induced CO_2 capture, release, and sequestration. Capture: $AQ + S_2O_4^{2-} + 2CO_2 + 2OH^- \rightarrow AQ(CO_2)_2^{2-} + 2HSO_3^-$ (step 1). Release: $AQ(CO_2)_2^{2-} + 2Fe(CN)_6^{3-} \rightarrow AQ + 2Fe(CN)_6^{4-} + 2CO_2\uparrow$ (step 2). Sequestration: $CO_2 + Ba(OH)_2 \rightarrow BaCO_3\downarrow + H_2O$ (step 3).

Step 1: with continuous CO_2 purging, the flask containing 0.1 M 1,8-BTMAPAQ, 1 M TBACl solution was added with a saturated aqueous solution containing two equivalents of NaOH and one equivalent of $Na_2S_2O_4$, forming the hemi carbonate $[AQ(CO_2)_2^{2-}]$.

Step 2: the solution was vigorously stirred in N_2 for 15 mins followed with 15-min N_2 purging.

Step 3: with continuous N_2 purging, the flask containing quinone solution was connected with another flask containing saturated $Ba(OH)_2$ solution prepared in advance under N_2. With N_2 purging, a saturated aqueous solution containing two equivalents of $K_4Fe(CN)_6$ was dropwise added to the quinone solution, generating CO_2 bubbles. The generated CO_2 was carried by N_2 to the $Ba(OH)_2$ flask, immediately forming cloudy $BaCO_3$.

The resulting suspension was centrifuged to collect the precipitates which were then dried in an oven completely until the dry mass becomes constant. The CO_2 capture capacity was calculated from the dry mass of $BaCO_3$. The power was cooled down in a desiccant then quickly weighed in a precision balance to obtain the dry mass.

BTMAPAQ chemical reduction/oxidation induced CO_2 capture/release followed with sequestration were designed to determine the carbon capture capacity. We found that one 1,8-BTMAPAQ molecule can capture and release two CO_2 molecules in the absence of oxygen.

Electrochemical CO_2 capture in O_2-free environment

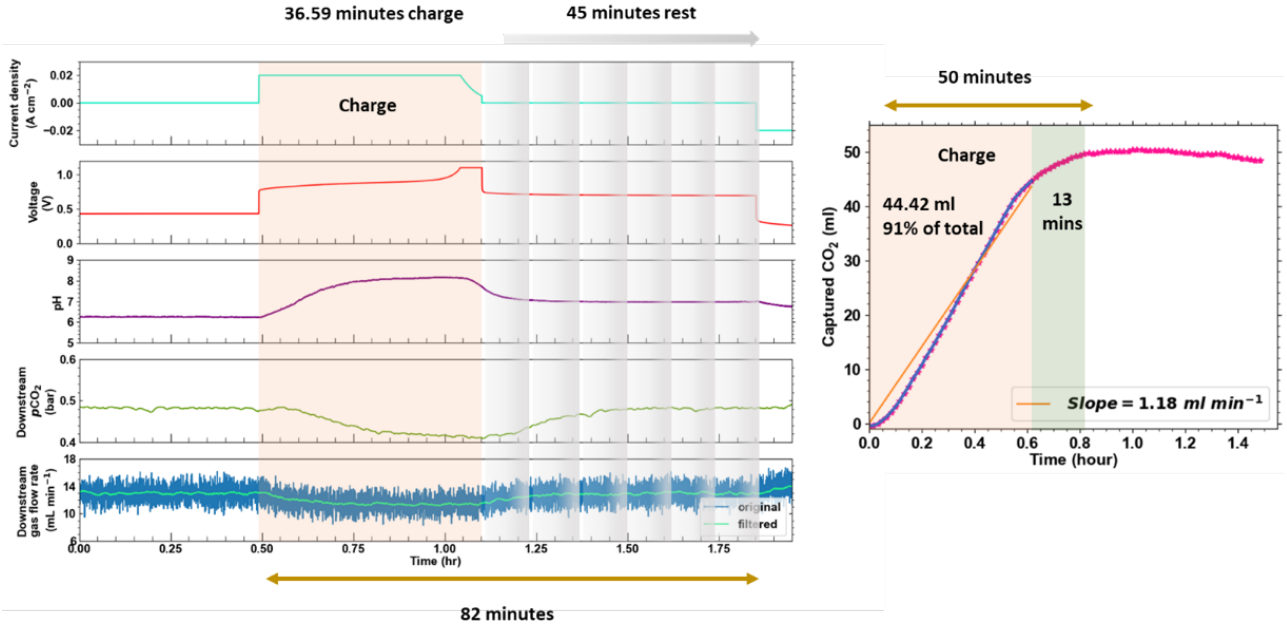

Figure S7 | Cumulative CO_2 captured during the charge and rest time for the fourth cycle of Figure 4a 0.5 bar CO_2 experiment. The figure demonstrates the total time needed for the complete capture of CO_2 for the conditions described in Figure 4a for the 0.5 bar CO_2 experiment.

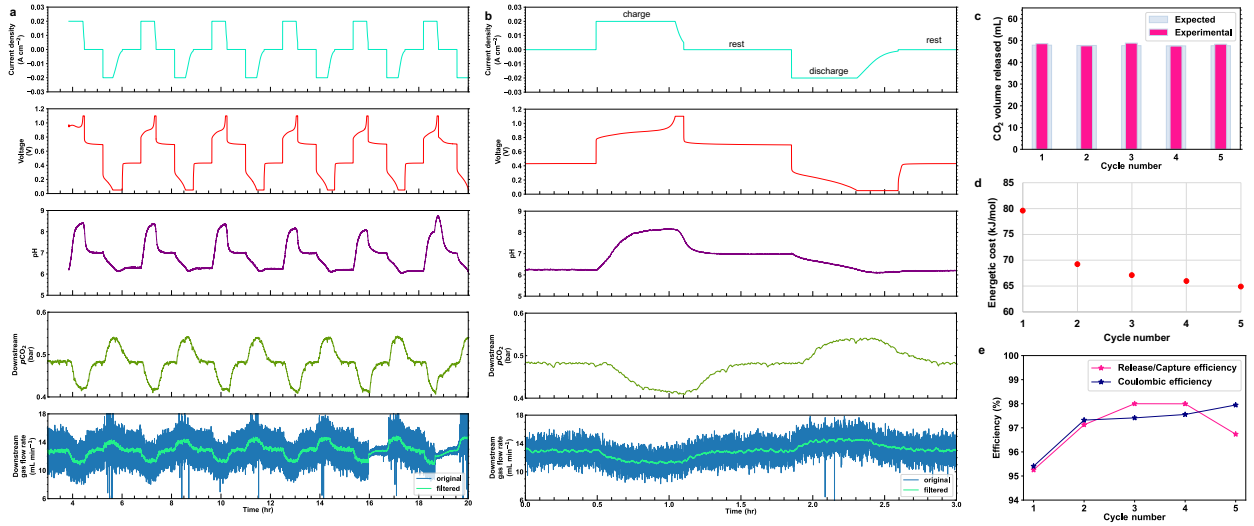

Figure S8 | CO_2 capture and release cycling in a flow cell comprising 10 mL of 0.115 M 1,5-BTMAPAQ in 1 M KCl (negolyte) and 40 mL of 0.1 M BTMAPFc in 1 M KCl (posolyte) at 20 mA/cm^2. The partial pressure of CO_2 is set to ≈0.5 bar throughout the experiment. Plot on the left (a) presents (from top to bottom): current density, voltage, pH of the negolyte, the percentage of N_2 and CO_2 in the upstream source gas, downstream CO_2 partial pressure and the downstream total gas flow rate. The initial gas flow rate is set to 11.76 mL/min. Plot on the right top (b) shows zoomed-in data of the fourth cycle. Plots on the bottom right (c) presents the volume of the CO_2 gas (in mL) calculated from the deviation from the baseline flow rate during the battery discharge and rest period. The second plot on the bottom right demonstrates the energy (d) required for each cycle of capture and release (kJ/mol) and the coulombic efficiencies (e) and release/capture efficiencies per cycle. Bis((3-trimethylammonio)propyl)ferrocene dichloride (BTMAPFc) was purchased from TCI-America chemical company.

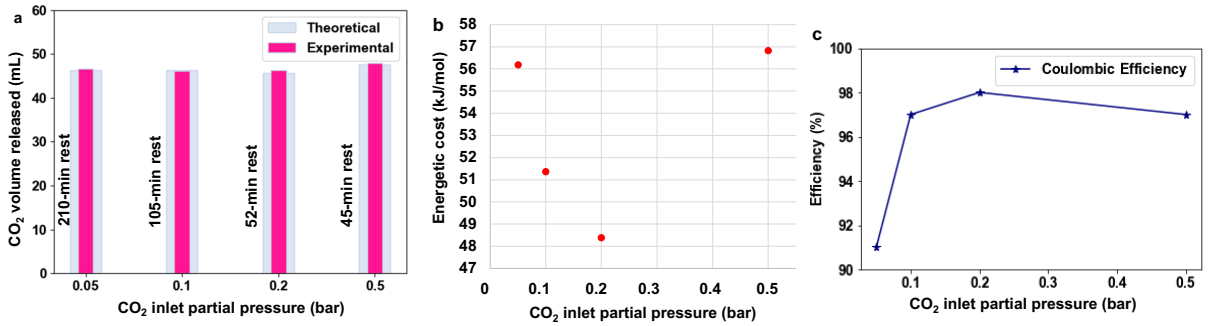

Figure S9 | CO_2 capture and release using different CO_2 partial pressure values in a flow cell comprising 12 mL of 0.115 M 1,5-BTMAPAQ in 1 M KCl (negolyte) and 40 mL of 0.2 M FcNCl in 1 M KCl (posolyte) at 20 mA/cm^2. The partial pressure of CO_2 is changing from 0.05 bar to 0.5 bar throughout the experiment. Plot on the top (a) shows the volume of the CO_2 gas (in mL) calculated from the deviation from the baseline flow rate during the battery discharge and rest period. The plot on the bottom demonstrates the average energy (b for 2 cycles) required for the capture and release of CO_2 and the coulombic efficiencies (c) using different CO_2 partial pressure values. Two CO_2 molecules were captured by one 1,5-BTMAPAQ with energetic cost of 48–57 kJ/molCO_2 at 20 mA/cm^2. (Ferrocenylmethyl)trimethylammonium Chloride (FcNCl) was purchased from TCI-America chemical company.

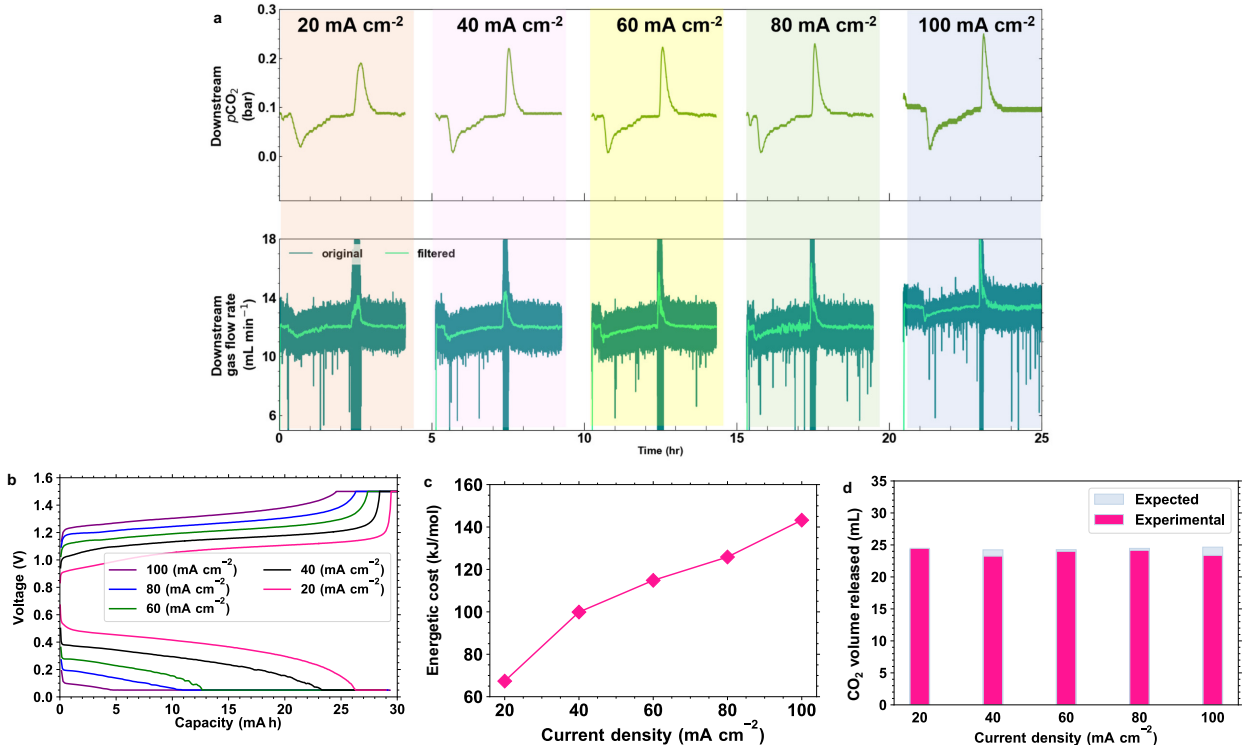

Figure S10 | CO_2 capture and release cycling at different current densities (20, 40, 60, 80, 100 mA/cm^2) in inlet CO_2 partial pressure of 0.1 and 0.5 bar in a flow cell comprising 10 mL of 0.057 M 1,5-BTMAPAQ in 1 M KCl (negolyte) and 40 mL of 0.2 M FcNCl in 1 M KCl (posolyte). Plot on the top left (a) presents the downstream CO_2 partial pressure and the downstream total gas flow rate. The initial gas flow rate is set to 11.76 mL/min. The plot on the top right (b) demonstrates the voltage versus capacity for each current density. (c) Plot shows the volume of the CO_2 gas (in mL) calculated from the deviation from the baseline flow rate during the battery discharge and rest period. (d) Plot shows the energetic cost of one charge and discharge per moles of released CO_2 for each current density tested.

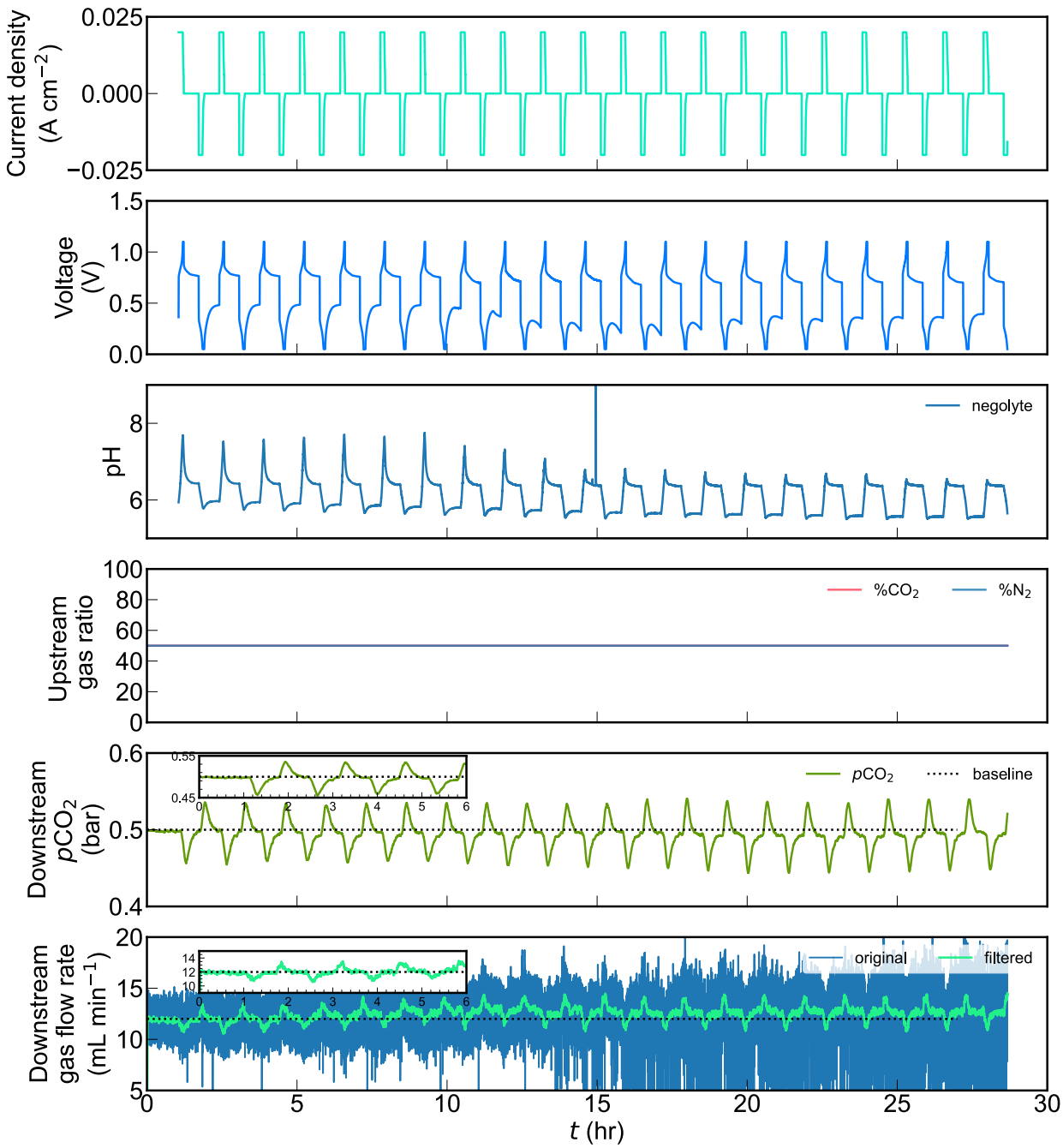

Figure S11 | CO_2 capture and release cycling at a current density of 20 mA/cm^2 in inlet CO_2 partial pressure of 0.5 bar in a flow cell comprising 10 mL of 0.057 M 1,5-BTMAPAQ in 1 M KCl (negolyte) and 40 mL of 0.2 M FcNCl in 1 M KCl (posolyte). Plots show the extended 21-cycle performance.

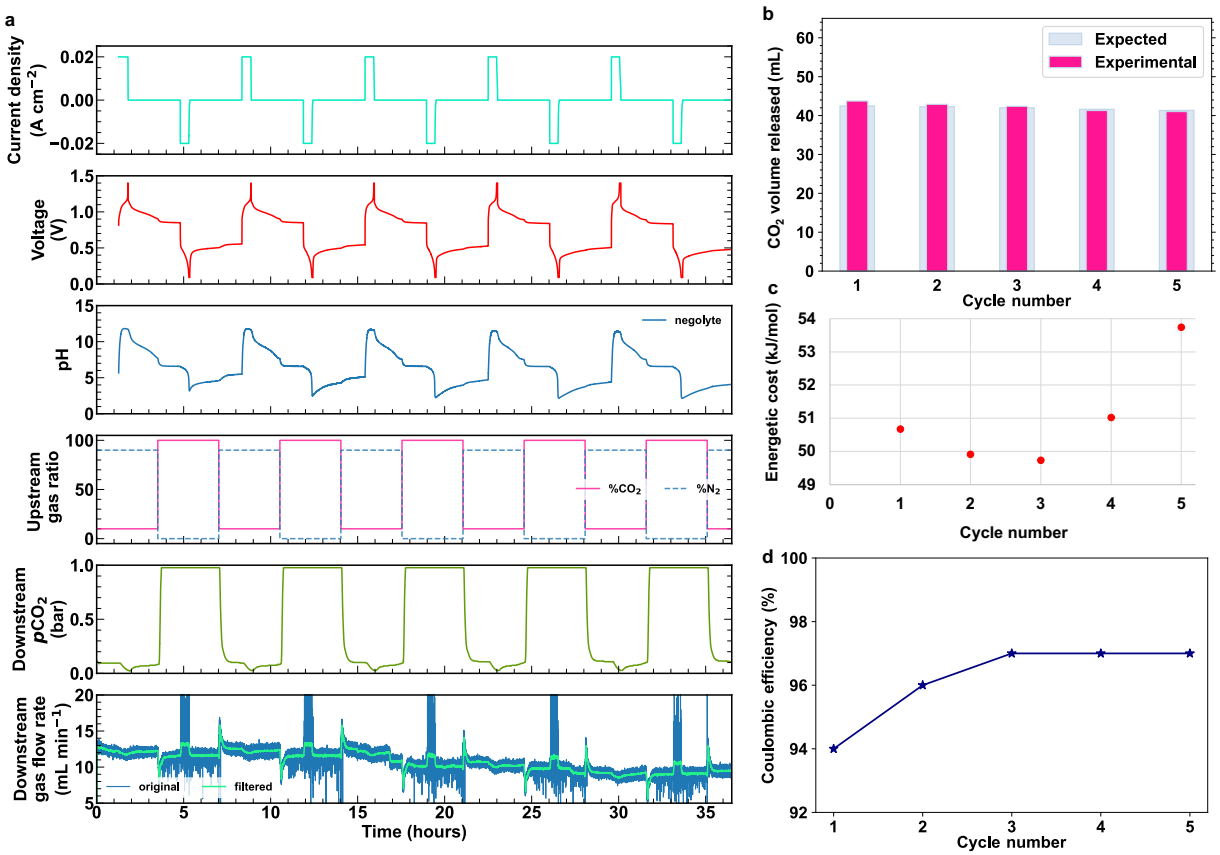

Figure S12 | CO_2 capture and release cycling where the capture occurs in an inlet CO_2 partial pressure of 0.1 bar and the release occur in an inlet CO_2 partial pressure of 1 bar in a flow cell comprising 12 mL of 0.115 M 1,5-BTMAPAQ in 1 M KCl (negolyte) and 40 mL of 0.2 M FcNCl in 1 M KCl (posolyte) at 20 mA/cm^2. Plot on the left (a) presents (from top to bottom): current density, voltage, pH of the negolyte, the percentage of N_2 and CO_2 in the upstream source gas, downstream CO_2 partial pressure and the downstream total gas flow rate. The initial gas flow rate is set to 11.76 mL/min. Plot on the right top (b) shows the volume of the CO_2 gas (in mL) calculated from the deviation from the baseline flow rate during the battery discharge and rest period. The plot on the bottom right demonstrates the energy (c) required for the capture and release of CO_2 in each cycler and the coulombic efficiency (d) for several cycles.

Concentrated cell test

A concentrated flow cell comprising 10 mL 0.4 M 1,5-BTMAPAQ and 40 mL 0.9 M FcNCl was assembled and tested. The cell was charged and discharged at 20 mA/cm^2 with no potential holds. The coulombic efficiency is 77% and the discharge capacity is 632.42 C. The experimental valume of released CO_2 is 148 mL which is close to the theoretical volume of released CO_2 (147 mL). The corresponding energetic cost is 90 kJ/molCO_2.

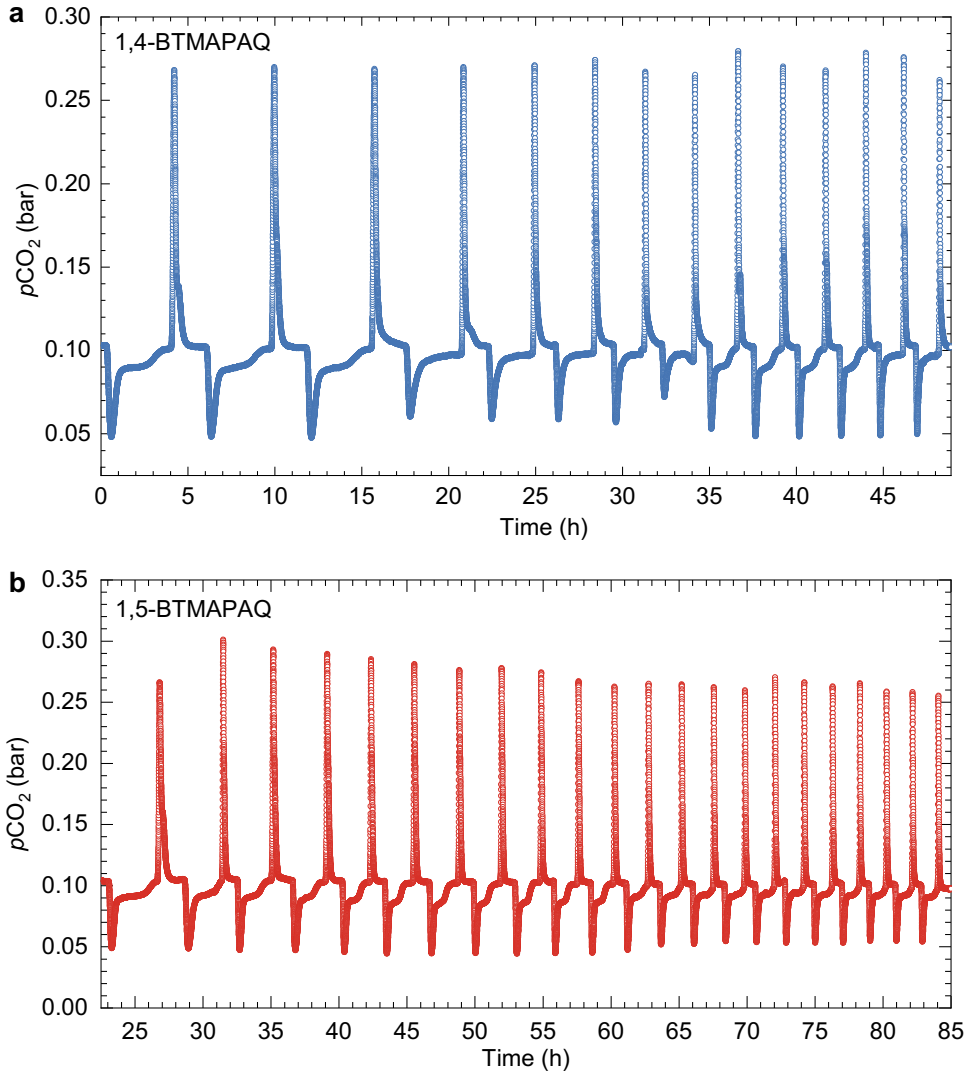

Figure S13 | CO_2 partial pressure changes over the electrochemical reduction and oxidation cycling of 1,4- and 1,5-BTMAPAQs. Electrolyte composition: 5 mL 0.1 M 1,4-, 1,5-BTMAPAQs, 1 M KCl vs. 40 mL 0.1 M FcNCl, 1 M KCl. Constant current (40 mA/cm^2) was followed with potential holds.

Oxygen sensitivity of reduced anthraquinones [H_2Q, HQ^-, Q^{2-}, $HQ(CO_2)^-$, and $Q(CO_2)_2^{2-}$]

CO_2 and O_2 account for ~10% and <5% in coal fired flue gas; ~0.04% (400 ppm) and 21% in air. Therefore, it is important to evaluate the oxygen effect of active species if were used for CO_2 capture.

Instead of exhaustively evaluating the oxygen sensitivity of each species, we mainly investigated two states, *i.e.*, fully reduced state with no chemisorbed CO_2 in which the most dominant and O_2-sensitive species is Q^{2-}; fully reduced state with chemisorbed CO_2 in which the most dominant species is $Q(CO_2)_2^{2-}$. The quinones in dissolved D_2O were chemically reduced and stored in air-tight J-Young NMR tubes, named as Q^{2-}; the quinones dissolved in D_2O were chemically reduced, introduced with CO_2, and stored in air-tight J-Young NMR tubes, named as $Q(CO_2)_2^{2-}$. The ^1H NMR spectra of two group samples were first collected in air-free environment. Subsequently, the samples were intentionally subject to air exposure, then tracked by ^1H NMR over the course of several days.

The oxygen sensitivity of 1,4-, 1,5-, 1,8-BTMAPAQ at states of Q^{2-} and $Q(CO_2)_2^{2-}$ was first evaluated by tracking their ^1H NMR followed with quantitative analyses of the aromatic peak areas in spectra. The ^1H NMRs of $Q(CO_2)_2^{2-}$ for AQDS, 2,6-D2PEAQ, and AQ-1,8-3E-OH were also tracked even though the use of tetra-alkyl ammonium salts to dissolve $Q(CO_2)_2^{2-}$ makes them unlikely to be used for electrochemical CO_2 capture. It is worth noting that exposing the reduced species in J-Young tubes to air is significantly different from practical application scenarios where huge amount of air would be vigorously pulled into electrolytes, we expect to extract the relative oxygen sensitivity trend from the comparison of those ^1H NMR spectra. The detailed analyses and comparison can be found below. Q^{2-} is generally more oxygen-sensitive than $Q(CO_2)_2^{2-}$, which is consistent with the right shifted anodic peaks observed in the CV results. Among the measured anthraquinones, 1,8-BTMAPAQ appears to be the least oxygen-sensitive, followed by 1,5- and 1,4-BTMAPAQ. Note that, 1 M TBACl was used for 1,8-BTMAPAQ electrolyte preparation, the resulting electrolyte become viscous, which might be the main reason being the least oxygen-sensitive. Molecular decomposition occurred in $1,8\text{-BTMAPAQ}^{2-}$, indicated by the appearance of side peaks over the course of air exposure.

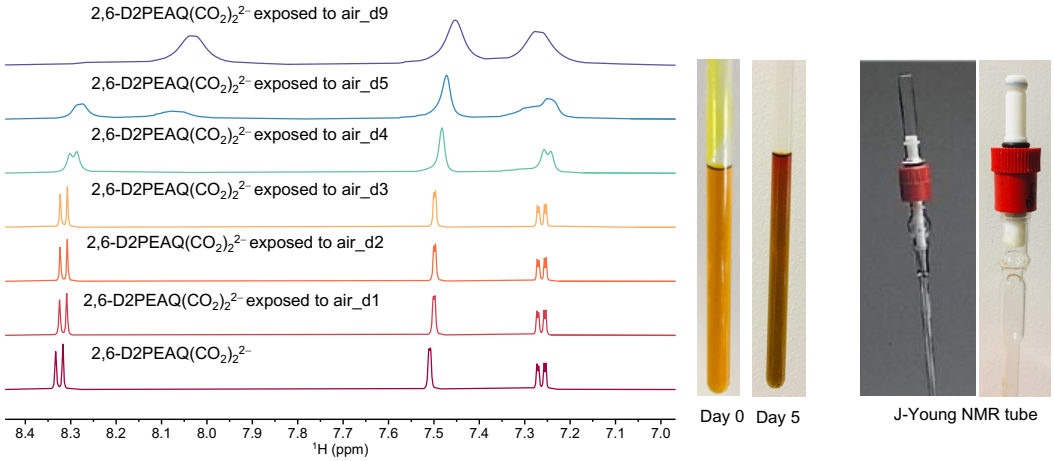

Figure S14 | ^1H NMR tracking of chemically synthesized 0.1 M $2,6\text{-D2PEAQ}(CO_2)_2^{2-}$ in 1 M TBABr D_2O over days while air was gradually introduced.

0.1 M $2,6\text{-D2PEAQ}^{2-}$ in 1 M tetra-n-butylammonium bromide (TBABr) D_2O solution was added to excess dry ice to form $2,6\text{-D2PEAQ}(CO_2)_2^{2-}$ and stored in a J-Young NMR tube. The ^1H NMR of $2,6\text{-D2PEAQ}(CO_2)_2^{2-}$ solution was periodically tracked over days. A tightly sealed J-Young NMR tube can well isolate the stored solution from air. One day-0, the ^1H NMR spectrum was taken in the air-tight J-Young NMR tube. From day-1, the red cap (shown in the pictures) was loosened and the white PTFE tip detached from the inner wall of the J-Young tube, allowing air to gradually diffuse into the solution and oxidize $2,6\text{-D2PEAQ}(CO_2)_2^{2-}$. As can be seen from the stacked ^1H NMR spectra, in the first three days, the aromatic peaks of $2,6\text{-D2PEAQ}(CO_2)_2^{2-}$ show clear splitting, indicating most of $2,6\text{-D2PEAQ}(CO_2)_2^{2-}$ remained intact; from day-4, the aromatic peaks became broader and shifted, which is be due to the occurrence of semi-radical anions, the partially oxidized species. $2,6\text{-D2PEAQ}(CO_2)_2^{2-}$ was gradually oxidized by molecular oxygen, forming oxidized species and hydroxide ions, which altered the pH of the solution. The color of the solution turned from bright yellow on day-0 to brown reddish on day-5 which is close to the color of the pristine 2,6-D2PEAQ solution (Figure 2a), implying that oxidation happened over the course of air exposure.

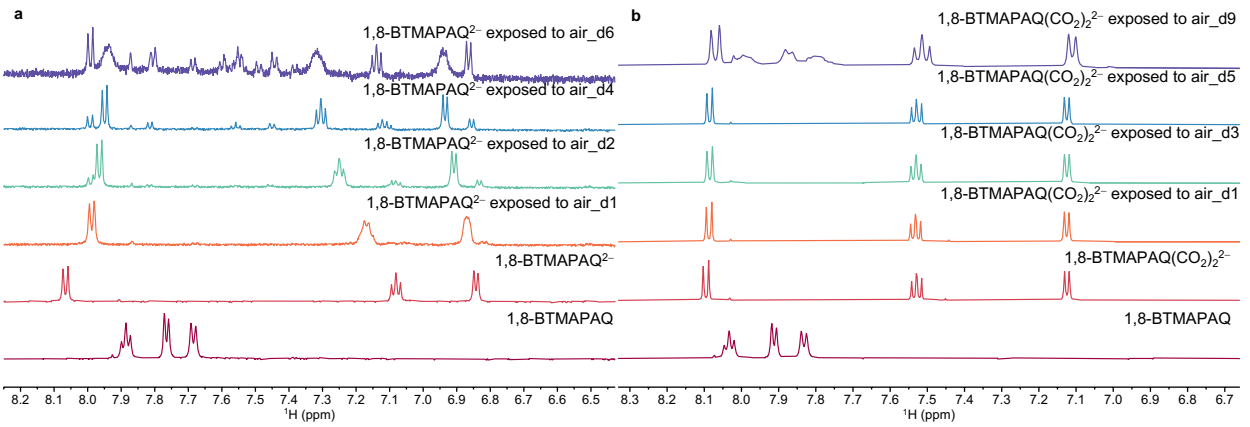

Figure S15 | ^{1}H NMR tracking of chemically synthesized 0.1 M 1,8-BTMAPAQ^{2-} (a) and 0.1 M 1,8-BTMAPAQ(CO$_2$)$_2^{2-}$ (b) in 1 M TBABr D$_2$O over days while air was gradually introduced.

0.1 M 1,8-BTMAPAQ, 1 M TBABr in D_2O was first chemically reduced by a stoichiometric amount of $Na_2S_2O_4$ with and without excess dry ice. The two samples were stored in two separate J-Young NMR tubes for day-0 tests. After that, the caps of J-Young NMR tubes were loosened up so that air can slowly diffuse into the solutions. The ^{1}H NMR spectrum of 0.1 M 1,8-BTMAPAQ was taken to serve as a control sample. On day-4 and day-6, some new peaks other than the peaks from 1,8-BTMAPAQ appear in the sample of 1,8-BTMAPAQ^{2-}, suggesting that 1,8-BTMAPAQ^{2-} is not structurally stable and molecular decomposition happened. On day-9, the sample of 1,8-BTMAPAQ(CO$_2$)$_2^{2-}$ showed the three sets of broad peaks between 7.7 ppm and 8.05 ppm which are similar to those in 1,8-BTMAPAQ, suggesting the hemi carbonate (quinone–CO_2 adduct) was slowly oxidized back to 1,8-BTMAPAQ.

As indicated in Figure 3a, the oxidation potentials of 1,8-BTMAPAQ^{2-} and 1,8-BTMAPAQ(CO$_2$)$_2^{2-}$ are –0.38 V and 0.12 V vs. SHE, which are lower than the reduction potential of O_2 (0.28 V vs. SHE) at pH 7. The relatively good oxygen resistance over days might be attributed to the addition of 1 M TBABr salt, which made the electrolyte more viscous, slowing down the dissolution of oxygen in the solution.

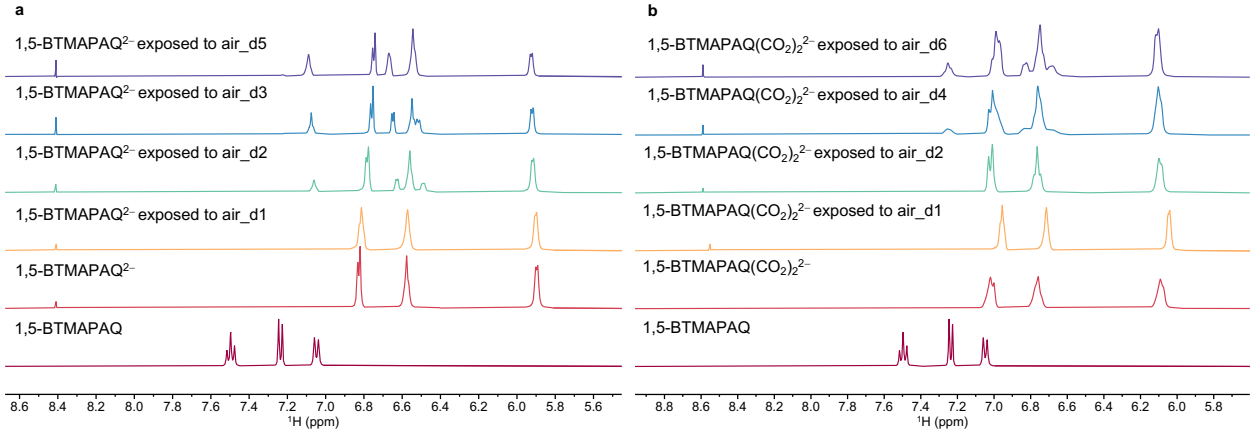

Figure S16 | ^{1}H NMR tracking of chemically synthesized 0.1 M 1,5-BTMAPAQ^{2-} (a) and 0.1 M 1,5-BTMAPAQ(CO$_2$)$_2^{2-}$ (b) in 1 M KCl D$_2$O over days while air was gradually introduced.

The 1,5-BTMAPAQ^{2-} and 1,5-BTMAPAQ(CO$_2$)$_2^{2-}$ were chemically synthesized and stored in J-Young NMR tubes by following the same methods described for the preparation of 1,8-BTMAPAQ^{2-} and 1,8-BTMAPAQ(CO$_2$)$_2^{2-}$. The only difference is using 1 M KCl as the supporting slat instead of 1 M TBABr. The former one is more preferred, as KCl is much smaller in size and much cheaper than tetra-alkyl ammonium salts.

After integrating the characteristic peak area from 1,5-BTMAPAQ, we found 23.6%, 37.0%, and 47.4% of 1,5-BTMAPAQ^{2-} were converted to the oxidized form on day-2, day-3, and day-5; whereas15.0% and 22.3% of 1,5-BTMAPAQ(CO$_2$)$_2^{2-}$ were converted to the oxidized form on day-4 and day-6, suggesting 1,5-BTMAPAQ^{2-} is more oxygen-sensitive than 1,5-BTMAPAQ(CO$_2$)$_2^{2-}$.

In Figure 3a, the oxidation potentials of 1,5-BTMAPAQ^{2-} and 1,5-BTMAPAQ$(CO_2)_2^{2-}$ are –0.38 V and 0.27 V vs. SHE, respectively. The latter one is quite close to the reduction potential (0.28 V vs. SHE) of O_2 at pH 7. It is thus reasonable to see good oxygen resistance from 1,5-BTMAPAQ$(CO_2)_2^{2-}$.

Unlike 1 M TBABr was used for 1,8-BTMAPAQ electrolytes, 1 M KCl was used for 1,5-BTMAPAQ electrolytes, the electrolytes have low viscosity and high oxygen solubility, that may explain why 1,5-BTMAPAQ^{2-} and 1,5-BTMAPAQ$(CO_2)_2^{2-}$ appear to be more oxygen sensitive than their 1,8-isomers (Figure S5).

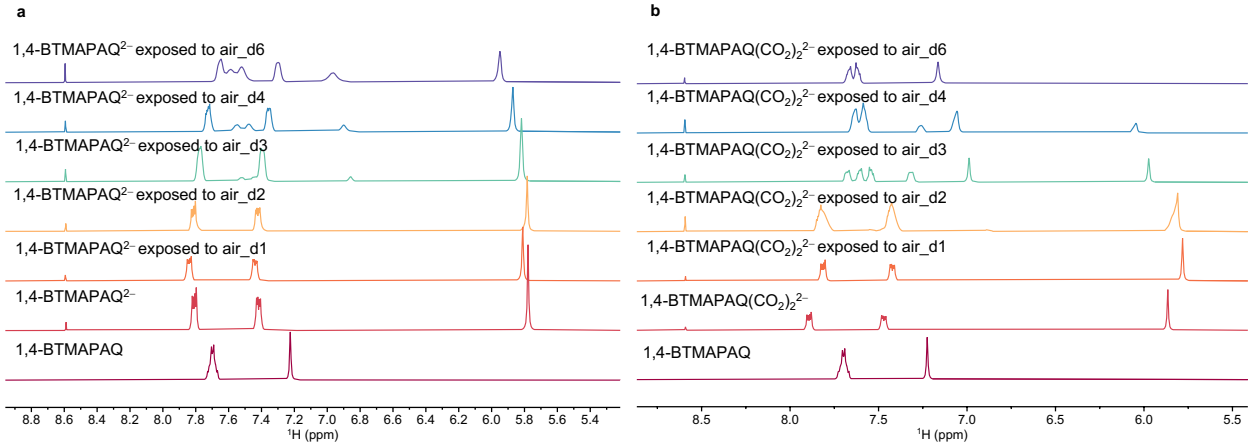

Figure S17 | ^{1}H NMR tracking of chemically synthesized 0.1 M 1,4-BTMAPAQ^{2-} (a) and 0.1 M 1,4-BTMAPAQ$(CO_2)_2^{2-}$ (b) in 1 M KCl D_2O over days while air was gradually introduced.

1,4-BTMAPAQ^{2-} and 1,4-BTMAPAQ$(CO_2)_2^{2-}$ were chemically synthesized and stored in J-Young NMR tubes by following the same methods described for the preparation of 1,5-BTMAPAQ^{2-} and 1,5-BTMAPAQ$(CO_2)_2^{2-}$.

After integrating the characteristic aromatic peak area from 1,4-BTMAPAQ, we found 11.3%, 27.6%, and 50% of 1,4-BTMAPAQ^{2-} was converted to the oxidized form on day-3, day-4, and day-6; whereas, 51.5%, 73.0%, and 98.0% of 1,4-BTMAPAQ$(CO_2)_2^{2-}$ was converted to the oxidized form on day-3, day-4, and day-6.

The oxidation potentials of 1,4-BTMAPAQ^{2-} and 1,4-BTMAPAQ$(CO_2)_2^{2-}$ are –0.36V and 0.23 V vs. SHE respectively; both are lower than the reduction potential of O_2 at pH 7. From the tracked ^{1}H NMR peak integral comparison, 1,4-BTMAPAQ$(CO_2)_2^{2-}$ seems to be more oxygen sensitive than 1,4-BTMAPAQ^{2-}, although the former one has a higher oxidation potential (Figure 3a). A plausible explanation is that reaction kinetics between 1,4-BTMAPAQ$(CO_2)_2^{2-}$ and O_2 is faster than the kinetics between 1,4-BTMAPAQ^{2-} and O_2.

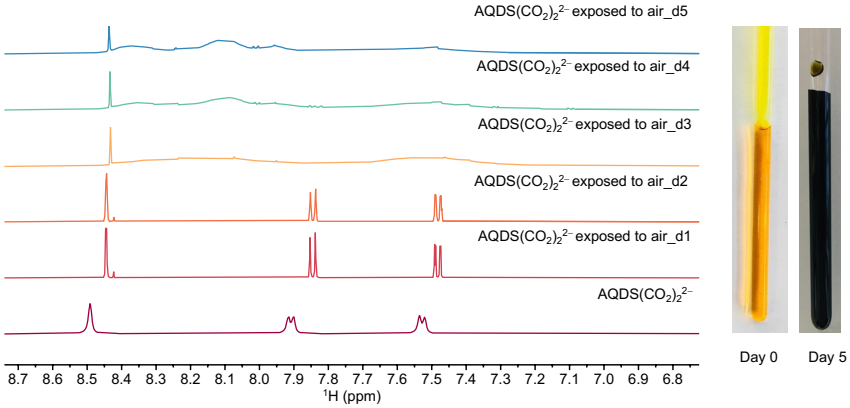

Figure S18 | ^{1}H NMR tracking of chemically synthesized 0.1 M AQDS$(CO_2)_2^{2-}$ in 1 M TMACl D_2O over days while air was gradually introduced.

The oxygen-sensitivity of 0.1 M AQDS$(CO_2)_2^{2-}$ in 1 M tetramethylammonium chloride (TMACl) D_2O solution was tracked by ^{1}H NMR periodically. The solution was prepared by mixing chemically prepared AQDS^{2-} with dry ice and stored in a J-Young NMR tube. The day-0 spectrum was taken in an air-tight J-Young NMR tube. From day-1, the cap was loosened, and air was gradually introduced to the solution. As shown in the stacked ^{1}H NMR spectra, the spectra maintained the same for the first two days, then the peaks become broader from day-3, indicating the coexistence of the oxidized, reduced, and intermediate states of AQDS. The color of the sample on day-5 became dark

green, as opposite to the bright yellow on day-0, suggesting that oxidation happened when the solution was exposed to air over days.

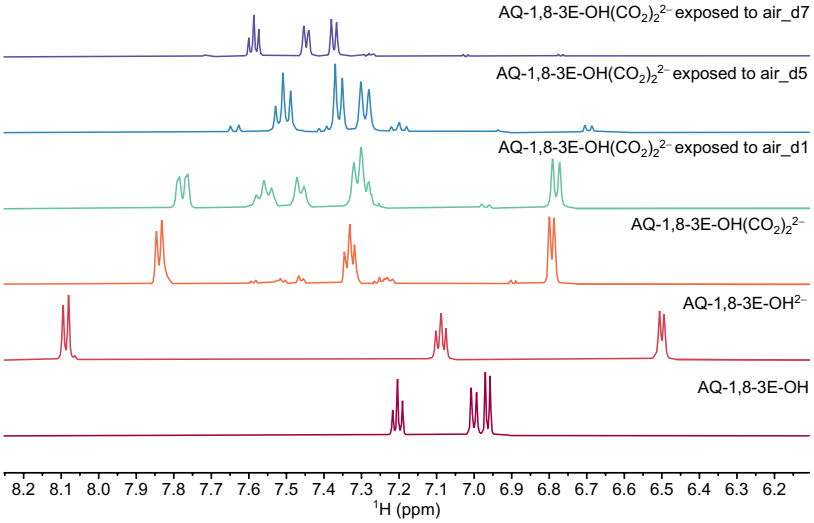

Figure S19 | ^{1}H NMR tracking of chemically synthesized 0.1 M AQ-1,8-3E-OH$(CO_2)_2^{2-}$ in 1 M TBABr D_2O over days while air was gradually introduced.
The oxygen sensitivity of 0.1 M AQ-1,8-3E-OH$(CO_2)_2^{2-}$ in 1 M TBABr D_2O solution was tracked by ^{1}H NMR periodically. As shown in the stacked ^{1}H NMR spectra, the bottom two are AQ-1,8-3E-OH and AQ-1,8-3E-OH^{2-}, respectivley. The AQ-1,8-3E-OH$(CO_2)_2^{2-}$ was stored in a regular NMR tube and tracked by ^{1}H NMR periodically. The regular NMR tube is not air-tight, and air can slowly diffuse to the solution. From day-1 to day-7, the peaks from AQ-1,8-3E-OH$(CO_2)_2^{2-}$ disappeared and instead the peaks of AQ-1,8-3E-OH showed up.

Table S2 | Coulombic efficiencies of BTMAPAQs | FcNCl flow cells while the BTMAPAQ electrolytes were kept in the atmosphere with different ratios of $O_2/CO_2/N_2$. Note that the BTMPAQ electrolytes were not stirred during the experiments. The anthraquinone electrolytes were just gently flushed by the 1 bar feed gas right above the liquid level.

BTMAPAQ	$O_2/CO_2/N_2$ (%)					
	0/0/100	0/10/90	2.1/10/87.9	5.25/10/84.75	10.5/10/79.5	18.9/10/71.1
1,4-	98.1%	90.3%	58.4%	52.1%	51.7%	44.9%
1,5-	97%	94%	82%	74.5%	60.6%	n/a
1,8-	98%	94%	85%	81%	79%	72%

Given that oxygen can chemically oxidize the reduced anthraquinones, the charge/discharge capacity of anthraquinone electrolytes will become higher/lower than theoretical capacity during charge/discharge processes in the presence of oxygen, thus lowering coulombic efficiencies (CE). Therefore, oxygen sensitivity of the reduced BTMAPAQs can be reflected by coulombic efficiency while varying the ratios of O_2 versus CO_2 in feed gas.

Table S1 lists coulombic efficiencies of 0.1 M 1,4-, 1,5-, 1,8-BTMAPAQ flow cells in the presence of different compositional feed gas. The cells were set to rest for **68 mins** under the feed gas exposure once they were fully charged. The supporting salt used for 1,4-, 1,5-BTMAPAQ is 1 M KCl; the supporting salt used for 1,8-BTMAPAQ is 1 M TBACl. Note that we did not stir the electrolytes to increase the contact area for the gas–liquid phase reactions, as we only aimed to extract the relative oxygen sensitivity trend of the three BTMAPAQs from their CE comparison.

Chemical CO_2 capture, release, and sequestration procedure in the presence of O_2

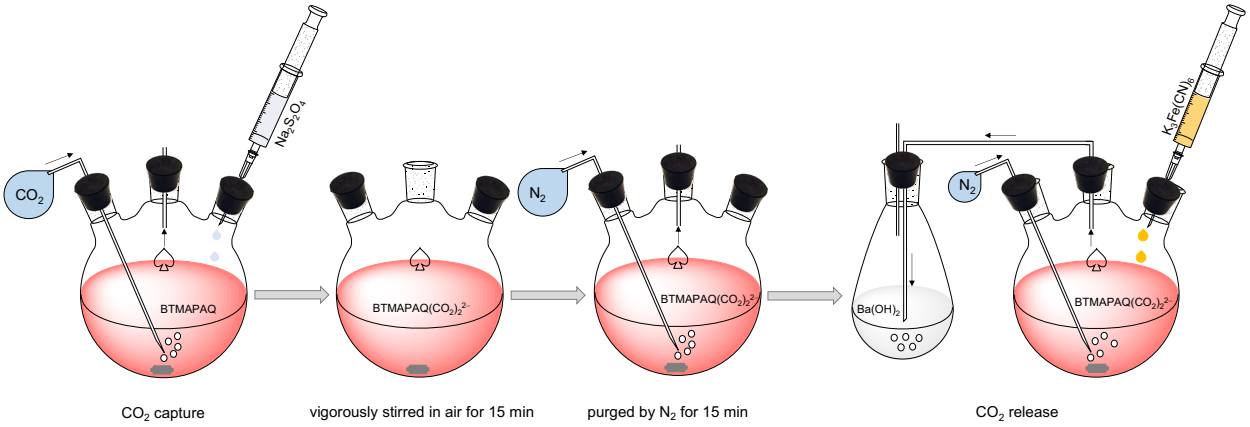

Figure S20 | Chemically induced CO_2 capture, release, and sequestration. Capture: $AQ + S_2O_4^{2-} + 2CO_2 + 2OH^- \rightarrow AQ(CO_2)_2^{2-} + 2HSO_3^-$ (step 1). Release: $AQ(CO_2)_2^{2-} + 2Fe(CN)_6^{3-} \rightarrow AQ + 2Fe(CN)_6^{4-} + 2CO_2\uparrow$ (step 2). Sequestration: $CO_2 + Ba(OH)_2 \rightarrow BaCO_3\downarrow + H_2O$ (step 3).
Step 1: with continuous CO_2 purging, the flask containing 0.1 M 1,8-BTMAPAQ, 1 M TBACl solution was added with a saturated aqueous solution containing two equivalents of NaOH and one equivalent of $Na_2S_2O_4$, forming the hemi carbonate $[AQ(CO_2)_2^{2-}]$.
Step 2: the solution was vigorously stirred in air for 15 mins followed with 15-min N_2 purging.
Step 3: with continuous N_2 purging, the flask containing quinone solution was connected with another flask containing saturated $Ba(OH)_2$ solution prepared in advance under N_2. With N_2 purging, a saturated aqueous solution containing two equivalents of $K_4Fe(CN)_6$ was dropwise added to the quinone solution, generating CO_2 bubbles. The generated CO_2 was carried by N_2 to the $Ba(OH)_2$ flask, immediately forming cloudy $BaCO_3$.
The resulting suspension was centrifuged to collect the precipitates which were then dried in an oven completely until the dry mass becomes constant. The CO_2 capture capacity was calculated from the dry mass of $BaCO_3$. The power was cooled down in a desiccant then quickly weighed in a precision balance to obtain the dry mass.

BTMAPAQ chemical reduction/oxidation induced CO_2 capture/release followed with sequestration were designed to determine the carbon capture capacity. We found that 1.7 CO_2 molecules on average were released when the CO_2 chemisorbed solution was stirred in air for 15 mins. 0.3 CO_2 per 1,8-BTMAPAQ was trapped in solution due to oxygen effect (see oxygen-involved side reactions in Table 1).

Electrochemical CO_2 capture in the presence of O_2

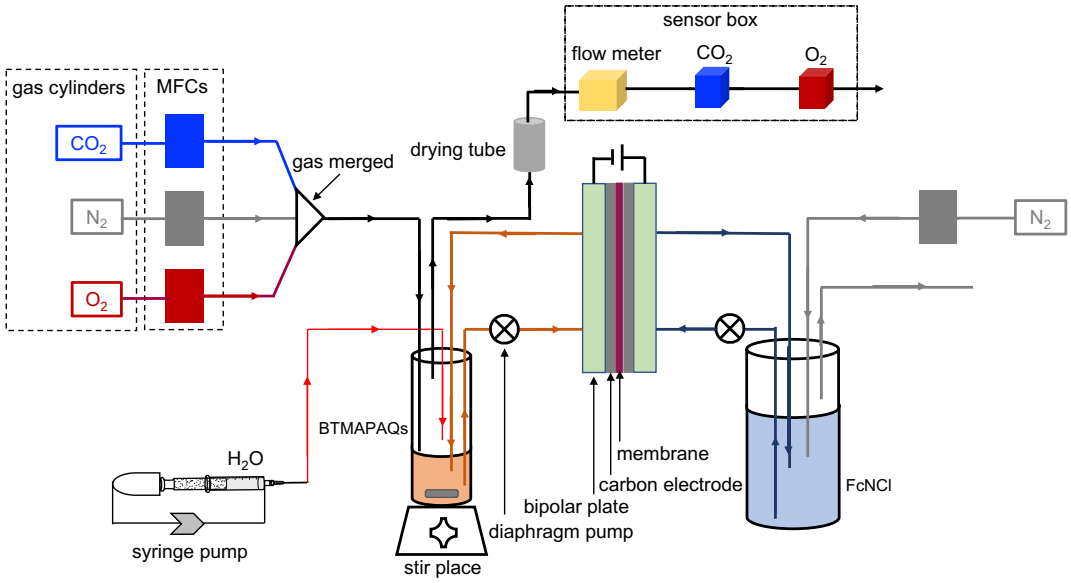

Figure S21 | Schematic of the electrochemical CO_2 setup in the presence of O_2.

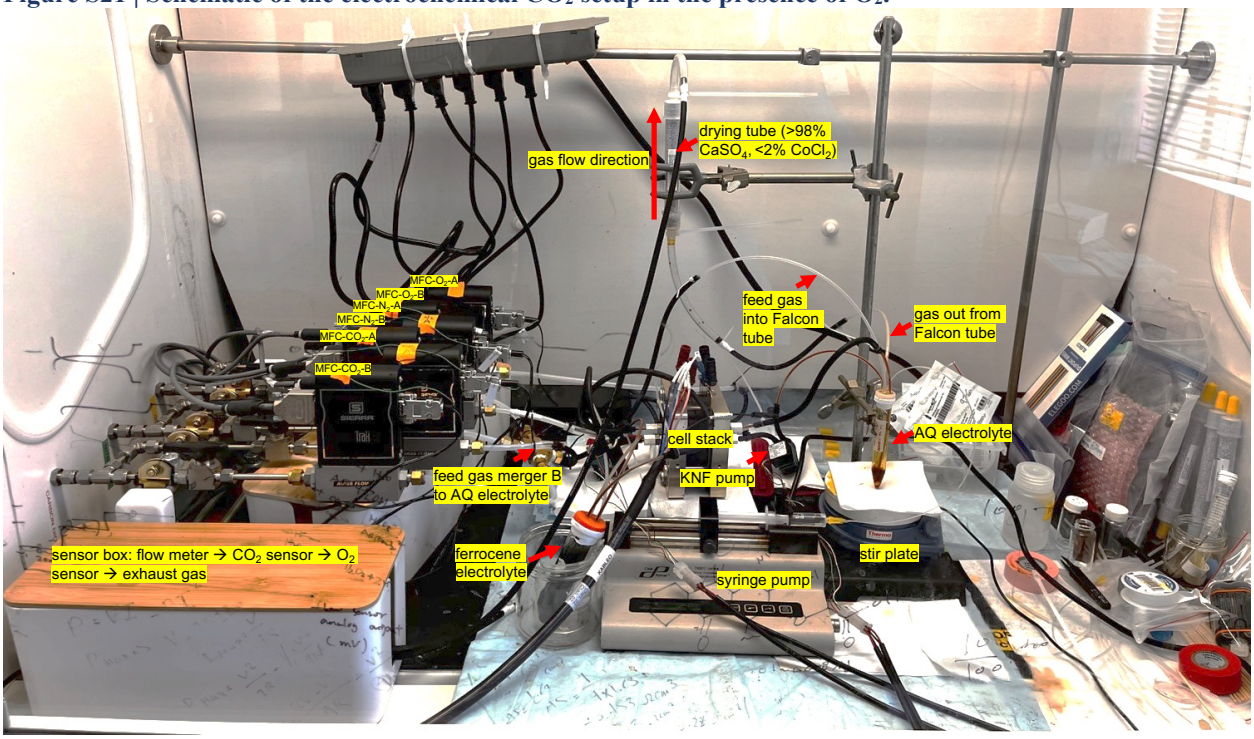

Figure S22 | Setup of electrochemical CO_2 capture with aqueous quinone flow chemistry. Mass flow controller (MFC) were controlled by Arduino UNO. MFC-O_2-A, MFC-N_2-A, and MFC-CO_2-A gas tubes were merged and introduced to the ferrocene electrolyte. MFC-O_2-B, MFC-N_2-B, and MFC-CO_2-B gas tubes were merged and introduced to the anthraquinone electrolyte.

FCT flow cell was used for the electrochemical tests. KNF diaphragm pumps were used to circulate electrolytes through the flow fields and electrodes in the cell stack. Unbaked AvCarb HCBA was used as electrodes. DSV-N was selected as the anion-exchange membrane. 15 mL and 50 mL Falcon tubes were choosen as anthraquinone and ferrocene electrolyte reserviors, respectively.

To avoid humidity interfering sensor detection, before gases flow into the gas sensors which are sitting in the sensor box, a drying tube full with >98% $CaSO_4$, <2% $CoCl_2$ is introduced to the gas line of anthraquinone electrolyte side.

A syringe pump was used to automatically compensate water loss due to the constant gas flow carring moisture out from the anthraquinone electrolytes.
A football-shape mini stir bar was added into the anthraquinone electrolyte reservior; under of which, a stir plate was placed to stir the electrolyte during the test to increase the contact area betetween liguid phase and gas phase.
FS4001 MEMS Mass Flow Sensor, LuminOX O_2 sensor (CM-42990), SprintIR CO_2 sensor (GC-0018) were used in our tests. Biologic SP-150e potentiostat was used as our electrochemical work station.
All of the sensors were calibrated prior to use. Because the partial pressure of the introcued O_2 to the system is only 0.03 bar, 3% of total pressure, 0.15 bar air was introduced and its flow rate was precisely controlled by the mass flow controller.

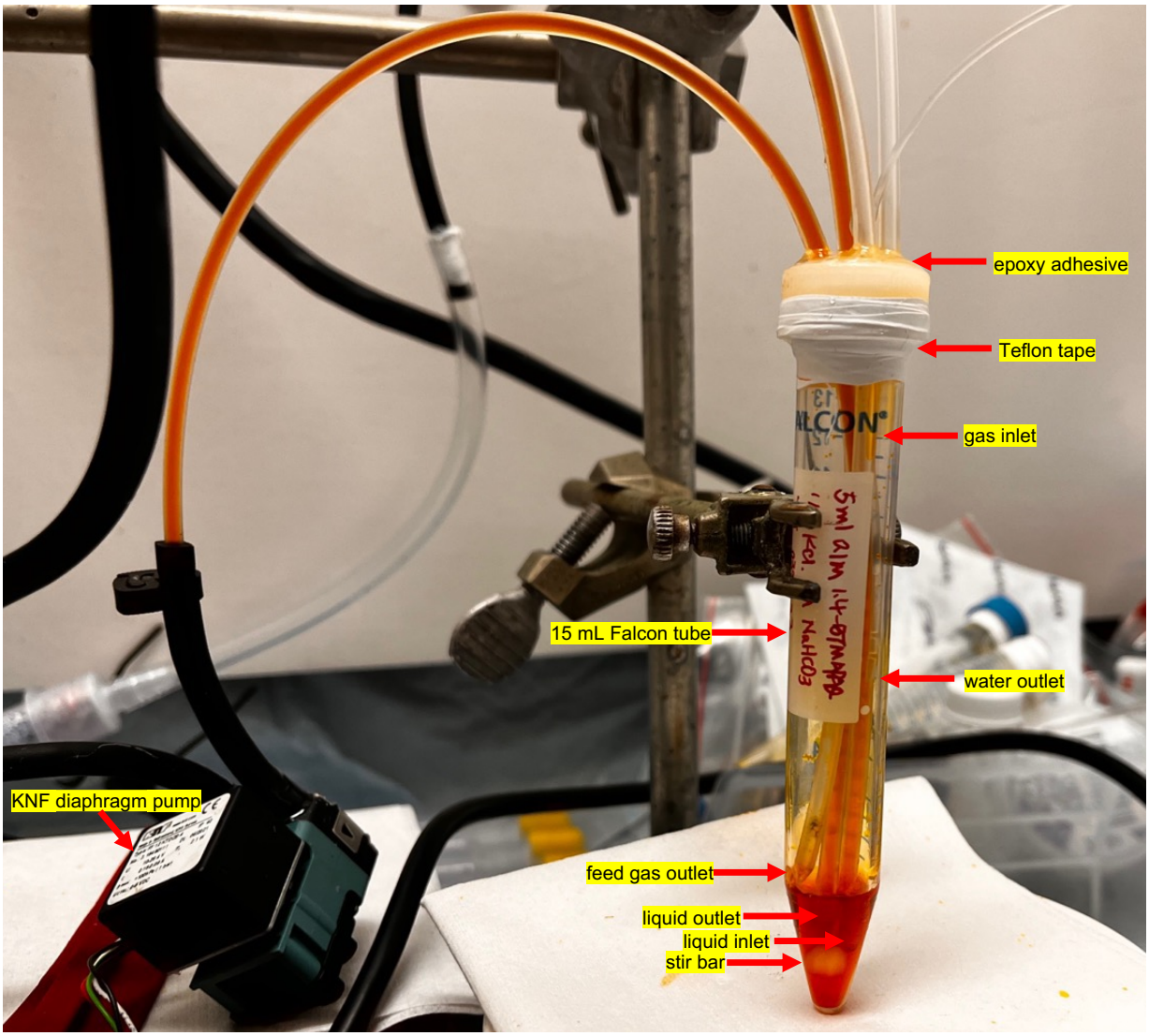

Figure S23 | A close look of tube positioning in the anthraquinone electrolyte Falcon tube. Epoxy was used to seal the holes on the cap to avoid any gas leakage.Telfon tape was also used to wrap around the joint of cap and tube body to prevent gas leaking.

The volume capacity of the Falcon tube accormodating the negative electrolytes is 15 mL. 5 mL BTMAPAQ electrolyte was usually prepared as the initial volume. Once being circulated through the cell stack, the remaining volume of BTMAPAQ electrolyte in the Falcon tube is 2 mL, leaving the headspace as 13 mL.
The volume capacity of the Falcon tube accormodating the positive electrolyte is 50 mL. 40 mL FcNCl electrolyte was usually prepared as the initial volume. Once being circulated through the cell stack, the remaining volume of FcNCl electrolyte in the Falcon tube is 37 mL, leaving the headspace as 13 mL.

The liquid flow rate of both positive and negative electrolytes was kept at 70 mL/min. The gas flow rate was kept at ~12 mL/min on both sides. Because of the constant gas purging, we set a syringe pump to automatically compensate the water loss in the negative electrolyte at a rate of 0.01 mL/h.
The viscosity of BTMAPAQ electrolytes is reasonably low and there is no mixing issue. A football shape magnatic stir bar with the dimension of ∅ 6 mm × 10 mm was used in the experiments. The stir rate was kept at 800 rpm, that kept whirling the electrolytes, accelerating the gas-liquid reaction.

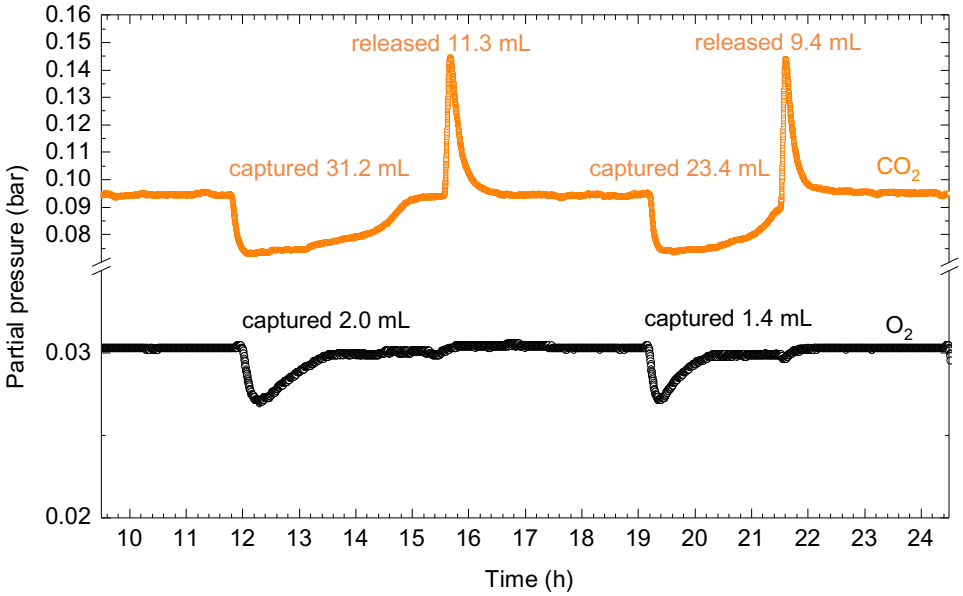

Figure S24 | Variation of CO_2 and O_2 partial pressure during the electrochemical reduction and oxidation of 1,5-BTMAPAQ electrolyte. A simulated flue gas composing of 3% O_2, 10% CO_2, and 87% N_2 was used as the feed gas stream and constantly introduced to the electrolyte. During and after the electrochemical reuduction, the reduced antrahquinone electrolyte became sensitive to O_2 and CO_2, causing the partial pressure drop for both of them. During the electrochemical oxidation, part of the captured CO_2 by the electrolyte was released, resulting in the CO_2 partial pressure increase. The integrated volumes of released CO_2 are smaller than those of captured CO_2, because oxygen-involved side reactions can irreversibly trap certain amount of CO_2, which cannot be released during the normal electrochemical oxidation.

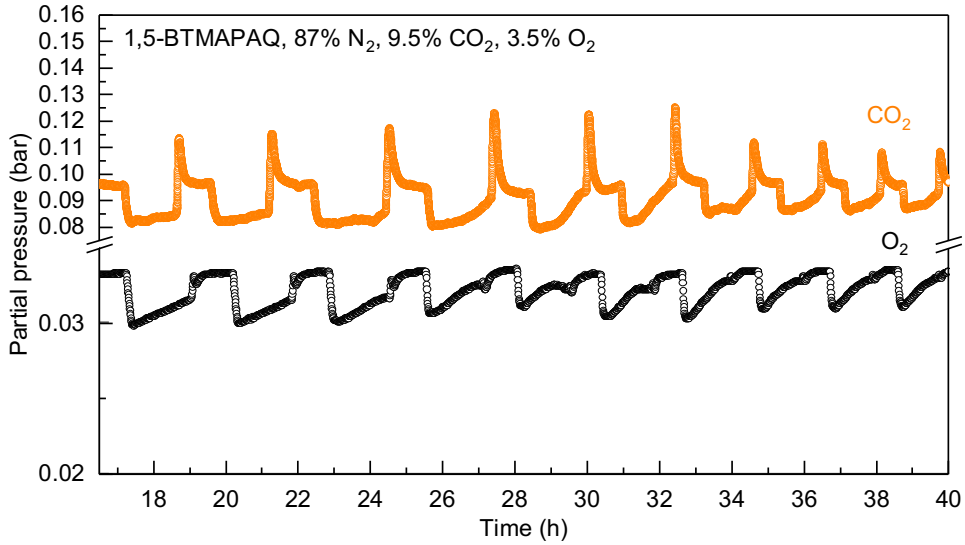

Figure S25 | Variation of CO_2 and O_2 partial pressure during the electrochemical reduction and oxidation of 1,5-BTMAPAQ in an one bar atmosphere of 87% N_2, 9.5% CO_2, and 3.5% O_2. Ideally, the O_2 partial pressure drop should align with the CO_2 partial pressure drop because the reduced anthraquinone can simutaneously react with CO_2 and O_2. The misalignment was caused by the CO_2 meter software artifact.

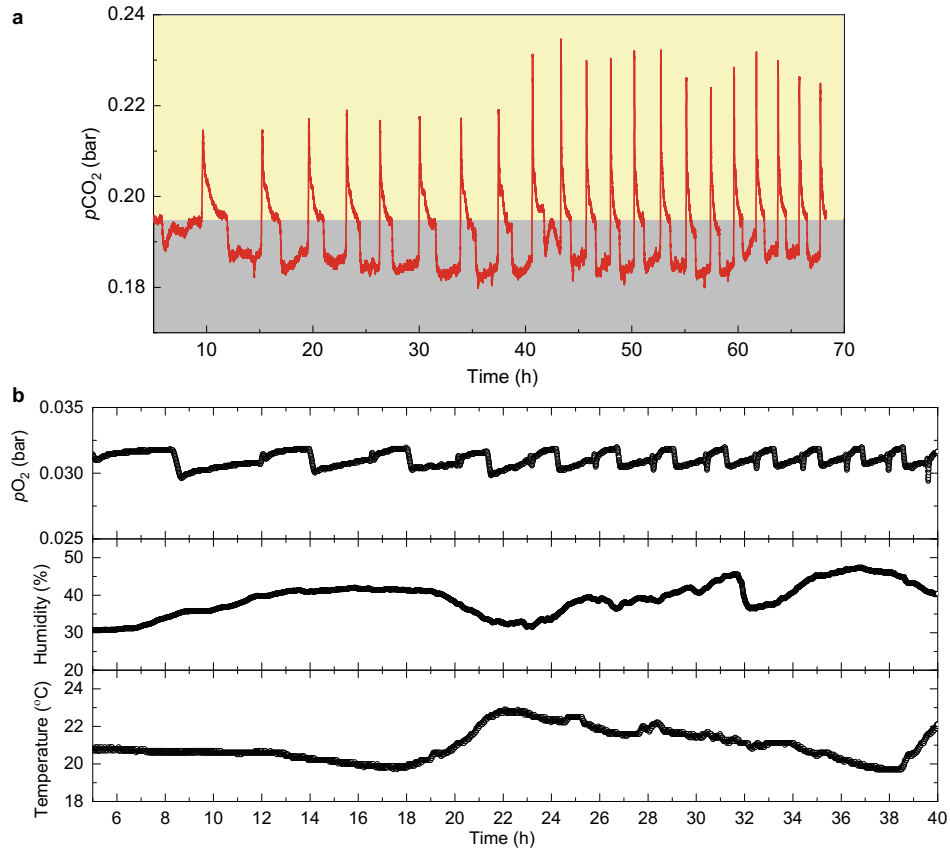

Figure S26 | Variation of (a) CO_2 and (b) O_2 partial pressure during the electrochemical reduction and oxidation of 1,5-BTMAPAQ in an one bar atmosphere of 77.4% N_2, 19.5% CO_2, and 3.1% O_2. The grey shade highlights the CO_2 capture; and the yellow shade highlights the CO_2 release. (b) Humidity and temperature were also recorded and tracked by the oxygen sensor.

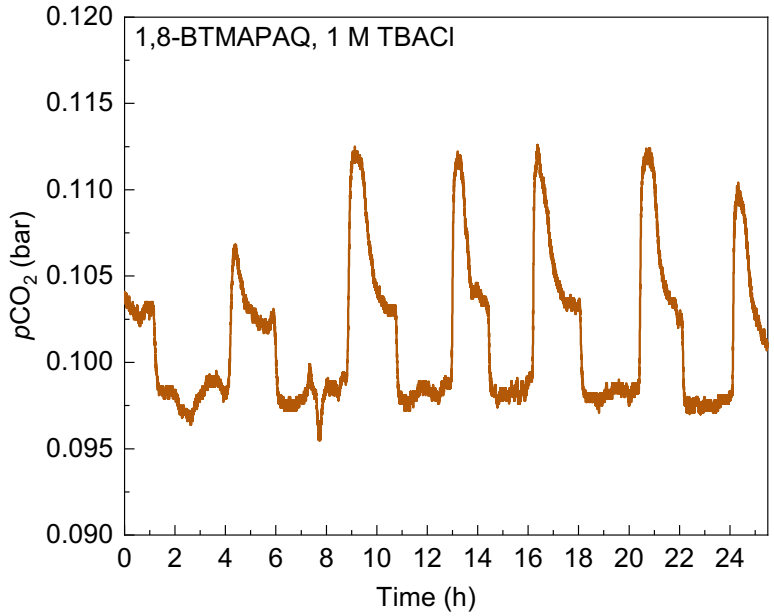

Figure S27 | Variation of CO_2 partial pressure during the electrochemical reduction and oxidation of 1,8-BTMAPAQ in an one bar atmosphere of 87% N_2, 10% CO_2, and 3% O_2.

References:

[1]Y. Zhu, Y. Li, Y. Qian, L. Zhang, J. Ye, X. Zhang, and Y. Zhao, "Anthraquinone-based anode material for aqueous redox flow batteries operating in nondemanding atmosphere", *Journal of Power Sources* **501**, (2021). https://doi.org/10.1016/j.jpowsour.2021.229984

[2]S. Jin, Y. Jing, D.G. Kwabi, Y. Ji, L. Tong, D. De Porcellinis, M.A. Goulet, D.A. Pollack, R.G. Gordon, and M.J. Aziz, "A water-miscible quinone flow battery with high volumetric capacity and energy density", *ACS Energy Letters* **4**, 1342 (2019). https://doi.org/10.1021/acsenergylett.9b00739

[3]E.F. Kerr, Z. Tang, T.Y. George, S. Jin, E.M. Fell, K. Amini, Y. Jing, M. Wu, R.G. Gordon, and M.J. Aziz, "High energy density aqueous flow battery utilizing extremely stable, branching-induced high-solubility anthraquinone near neutral pH", *ACS Energy Letters* **8**, 8 (2023). https://doi.org/https://doi.org/10.1021/acsenergylett.2c01691